further inserted into a modified *pRosa26-1* vector, which contains *Rosa26* genomic sequences.[21] Finally, the entire fragment was introduced into murine ES cells by electroporation. Southern blotting analysis and genomic PCR confirmed the correct homologous recombination, and the resultant clones were used to generate germline chimeras and heterozygous mice (Figure 1, B and C). All of the heterozygous mice were apparently normal and fertile. These mice did not express *Flag-Notch2* (Supplementary Figure 1), suggesting that there was no leaked expression of Notch2 in the absence of Cre recombinase activity.

Overexpression of *Notch2* in Embryonic Nephron Progenitors Leads to Severe Dysgenesis

To gain insights into the roles of Notch2 in renal progenitors, we crossed *R26Notch2* mice with *Six2Cre* mice specifically expressing Cre recombinase in renal progenitor populations in the metanephric mesenchyme (kindly provided by Dr. A.P. McMahon, Harvard University).[11] The resulting *Six2Cre/R26Notch2* mice were born at Mendelian frequency, but all of them died shortly after birth and displayed severe reductions in their kidney sizes (Figure 2, A and B). Histologic examination revealed that the mutant kidneys contained multiple glomerular cysts, dilated renal tubules, and thin cortexes (Figure 2, C and D). Some of the dilated tubules were positive for a proximal tubule marker, although it was not overproduced as observed for Notch1 activation when the same Cre line was used to ectopically express the intracellular domain of Notch1 in metanephric mesenchyme.[18] These results suggest that, unlike Notch1 activation, Notch2 activation does not drive the cell fate toward the proximal nephron but leads to severe dysgenesis.

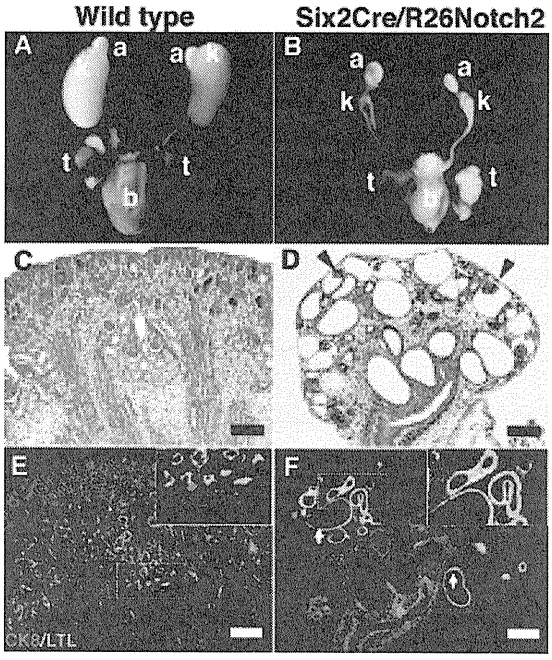

Figure 2. Overexpression of *Notch2* in embryonic nephron progenitors leads to severe kidney dysgenesis. (A) Kidneys in a newborn wild-type mouse (P0). k, kidney; t, testis; b, bladder; a, adrenal gland. (B) Kidney size is reduced in a newborn *Six2Cre/R26Notch2* mouse (P0). (C and D) HE staining of newborn kidneys. Severe dysgenesis is observed in the *Six2Cre/R26Notch2* kidney. Arrowheads show glomerular cysts. (E and F) Immunostaining for *Lotus tetragonobulus* lectin (LTL; green; proximal tubule marker) and cytokeratin 8 (CK8; red; ureteric bud marker). The upper right panels show higher-magnification images of the dotted square regions. They are ×2 of the original panels. Proximal tubules are not overproduced under Notch2 activation. Arrows, dilated proximal tubules. Scale bar = 100 μm.

Notch2 Overexpression Causes Nephron Progenitor Depletion

At embryonic day 14.5 (E14.5) during gestation, the mutant kidneys were already reduced in size and showed a thin cortical nephrogenic zone and poor nephron development (Figure 3, A and B). Immunostaining confirmed these findings. Although condensed metanephric mesenchyme (Pax2 positive/cytokeratin negative) surrounded the ureteric buds (Pax2 positive/cytokeratin positive) in the wild-type cortex accompanied by more differentiated Pax2-positive tubules, the mutant kidneys completely lacked the cortical mesenchyme and contained only small numbers of Pax2-positive scattered tubules (Figure 3, C–F). Ureteric branching was also impaired, and no ureteric bud-derived epithelia were observed in the mutant cortex (Figure 3, E and F). Consistent with these observations, the specific expression of Six2 in the nephron progenitors was significantly reduced in the mutant kidneys (Figure 3, G and H). Expression of Sall1, another marker for the progenitors, was also decreased in the mesenchyme, whereas its expression in the stroma was unaffected (Figure 3, I and J). Furthermore, *Foxd1*, a specific marker for the stroma, was also unaffected (Figure 3, K and L), reflecting the restricted activity of Cre recombinase in the mesenchyme but not in the stroma. These data suggest that *Notch2* overexpression in the metanephric mesenchyme leads to nephron progenitor depletion.

Notch2 Overexpression Leads to Ectopic *Wnt4* Expression and Premature Tubule Formation

During normal development at E12.5, Six2 was expressed in the dorsal (outer) domain of the mesenchyme against the ureteric buds, whereas *Wnt4* was expressed in the ventral (inner) domain to play an essential role in epithelial conversion of the mesenchyme (Figure 4, A and C). In the *Notch2*-activated mutant mice, Six2 expression was reduced, and *Wnt4* was detected in the mesenchyme all around the ureteric buds (Figure 4, B and D), indicating that *Wnt4* was ectopically expressed in the dorsal domain, which could accelerate the epithelial conversion of the otherwise undifferentiated nephron progenitors. Indeed, this notion was confirmed by double staining of laminin and cytokeratin at E14.5 (Figure 4, E–H). In the control mice, newly formed tubules of mesenchymal origin (laminin positive/cytokeratin negative) were located in close contact with and ventral to the cortical ureteric buds (laminin positive/

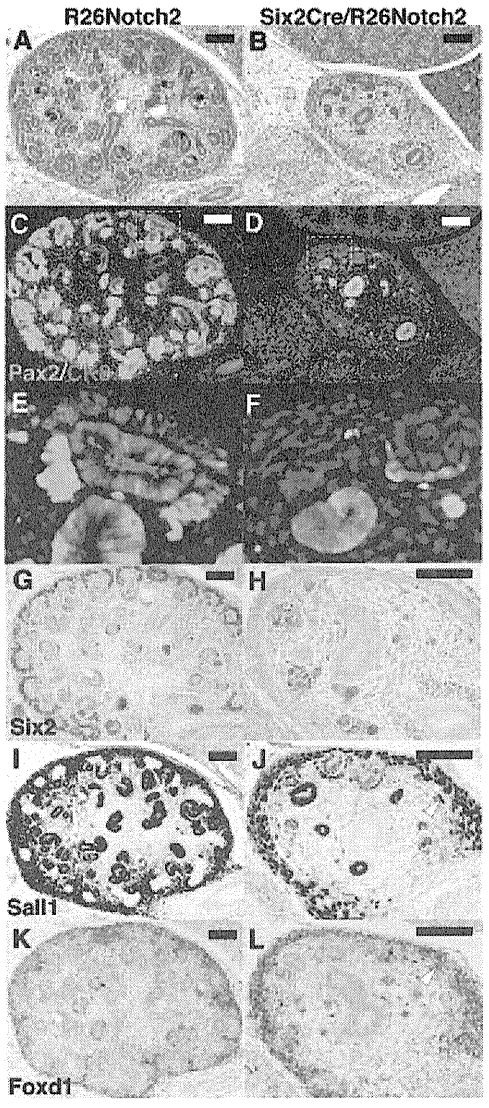

Figure 3. Notch2 overexpression causes nephron progenitor depletion. (A and B) HE staining at E14.5 during gestation. The mutant kidney is reduced in size and shows a thin cortical nephrogenic zone and poor nephron development, compared with the control kidney (*R26Notch2*). (C and D) Immunostaining for Pax2 (green) and cytokeratin 8 (CK8; red). (E and F) Higher-magnification images of the dotted square regions in panels C and D. They are ×6 of the panels C and D. Pax2-positive/cytokeratin-negative cells (arrowhead) that surround the ureteric bud-derived epithelia (arrow) are missing in the mutant cortex. Ureteric branching is also impaired. (G and H) Six2 immunostaining is significantly reduced in the mutant cortex. (I and J) Immunostaining of Sall1. Mesenchymal expression of Sall1 is reduced in the mutant kidney, whereas its stromal expression is retained (arrowhead). (K and L) *In situ* hybridization of *Foxd1*, a stromal marker. *Foxd1* continues to be expressed in the mutant kidney (arrowhead). Scale bar = 100 μm.

cytokeratin positive). In contrast, the tubules in the mutant mice were observed dorsal to poorly branched ureteric buds that failed to develop into the cortex (Figure 4, G and H). Pax2 and cytokeratin staining further confirmed these results (Figure 2, C–F). As expected, all of the mesenchyme-derived epithelia in the mutants, including the renal tubules and glomerular podocytes but not the ureteric buds, overexpressed the intracellular domain of *Notch2* (Figure 4, I and J, and Supplementary Figure 2, A and B). Even some of the dilated cystic epithelia continued to express the exogenous Notch2 (Supple-

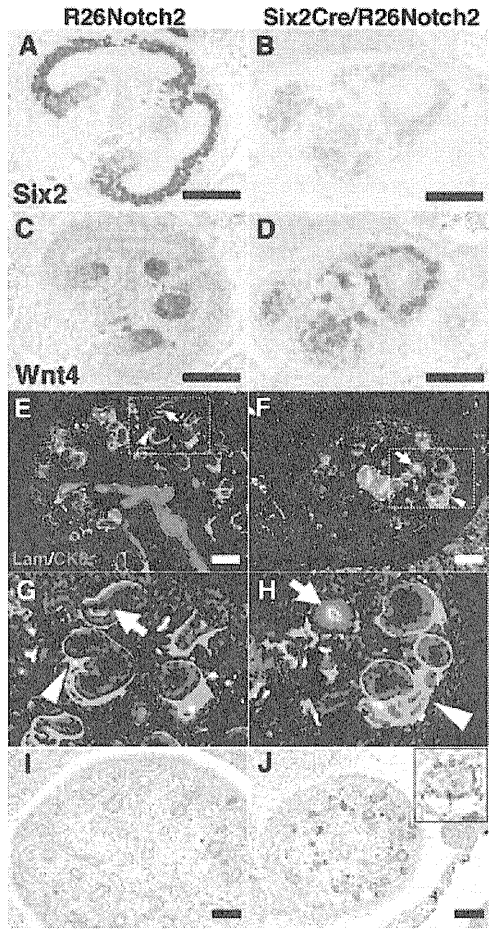

Figure 4. Notch2 overexpression leads to ectopic *Wnt4* expression and premature tubule formation. (A) Immunostaining of Six2. Six2 is expressed dorsally to the ureteric buds in the control kidney (*R26Notch2*) at E12.5. (B) Six2 immunostaining is reduced in the *Six2Cre/R26Notch2* kidney. (C) *In situ* hybridization of *Wnt4*. *Wnt4* is expressed ventrally against the ureteric buds in the control kidney at E12.5. (D) *Wnt4* expression is not confined to the ventral side of the ureteric buds in the *Six2Cre/R26Notch2* kidney. (E) Immunostaining for laminin (Lam; green; epithelial marker) and cytokeratin 8 (CK8; red; ureteric bud marker). Mesenchyme-derived tubules (arrowhead) are formed ventrally to the cortical ureteric bud-derived epithelia (arrow) in the control kidney at E14.5. (F) Ectopic tubules (arrowhead) are observed dorsal to the poorly branched ureteric bud-derived epithelia (arrow). Scale bar = 100 μm. (G and H) Higher-magnification images of the dotted square regions in panels E and F. They are ×3 of the panels E and F (I and J) *In situ* hybridization of the intracellular domain of *Notch2*. Note that all of the mesenchyme-derived epithelia in the mutants express *Notch2* (J). The upper right panel in J shows a higher-magnification image of glomerular podocytes. I and J are taken at ×100, and the inset is taken at ×400.

mentary Figure 2, C and D). These data indicate the occurrence of ectopic and premature epithelialization of the nephron progenitors, which could be the primary cause of the progenitor depletion. These phenotypes are very similar to those of *Six2*-deficient mice,[13] further supporting that Notch2-mediated Six2 suppression is a key molecular event that leads to progenitor depletion.

Pax2 Is Reduced and *Hesr1/Hesr3* Are Increased in Notch2 Activation

Next, we investigated molecules that could be responsible for the Six2 suppression by Notch2. At E11.5, the mutant kidneys were histologically indistinguishable from the control kidneys (Figure 5, A and B). No significant differences in proliferation and apoptosis were observed in the mesenchyme at E11.5 (Supplementary Figure 3). However, Six2 expression was already reduced, and the *Wnt4* domain had expanded dorsally (Figure 5, C–F). Pax2, Eya1, and Hox11 are known to bind to the *Six2* promoter and directly regulate *Six2* expression.[14] Under Notch2 activation, the expression of Pax2 in the mesenchyme was reduced, whereas those of *Eya1* and *Hoxd11* remained unaffected (Figure 5, G–J, and data not shown). *Gdnf*, another direct target of the Pax2/Eya1/Hox11 complex, was also decreased in the mutant kidneys (Figure 5, K and L), which could explain the reduced branching of the ureteric buds. In contrast, Sall1 and *Wt1* were minimally affected (Figure 5, M–P). Quantitative RT-PCR revealed similar tendencies (Figure 5Q). *Six2* was reduced and *Wnt4* was upregulated. A slight reduction in *Pax2* was also observed, despite the fact that it was also expressed in the ureteric buds. There were no significant changes in *Eya1* or *Hoxd11*, both of which were expressed in the mesenchyme. These data suggest that Notch2-dependent Six2 suppression could be mediated by inhibition of Pax2 expression. Other possibilities are described in the Discussion section.

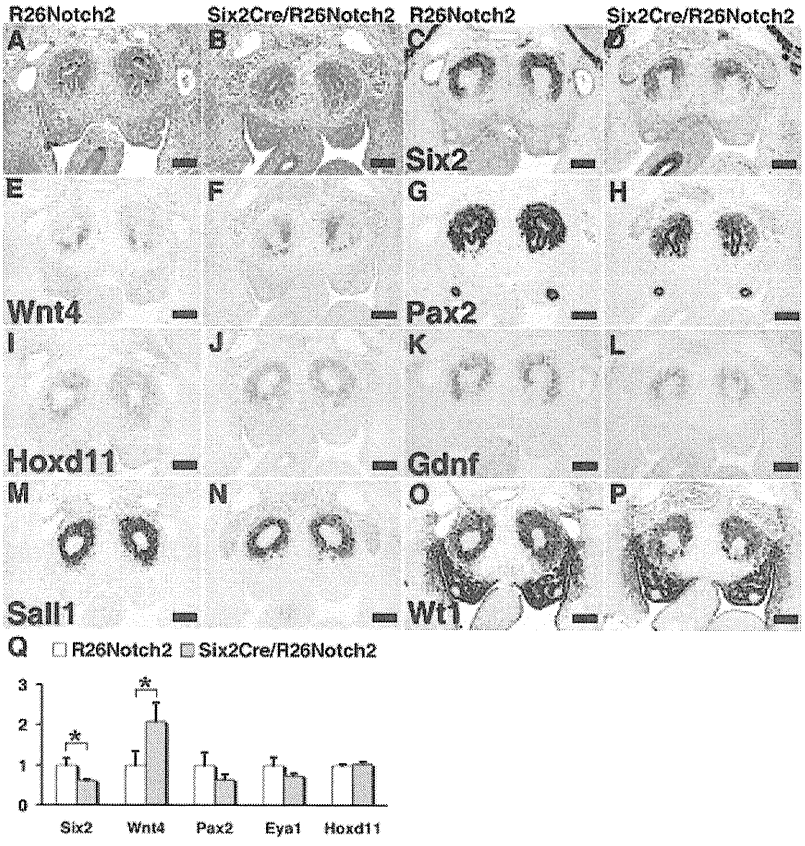

Figure 5. Expression of Pax2 is impaired under Notch2 activation. (A) HE staining of a control kidney (*R26Notch2*) at E11.5. The ureteric bud invades into the mesenchyme. (B) HE staining of a *Six2Cre/R26Notch2* kidney at E11.5. The mutant kidney is indistinguishable from the control kidney. (C and D) Six2 staining is reduced in the mutant mesenchyme. (E and F) *In situ* hybridization of *Wnt4*. The *Wnt4* expression domain is expanded dorsally in the mutant kidney. (G and H) Pax2 staining in the mesenchyme is reduced in the mutant kidney, whereas its expression in the ureteric bud is unaffected. (I and J) *In situ* hybridization of *Hoxd11*. *Hoxd11* expression is unaffected in the mutant kidney. (K and L) *In situ* hybridization of *Gdnf*. *Gdnf* expression is reduced in the mutant kidney. (M and N) Sall1 staining is minimally affected in the mutant kidney. (O and P) Wt1 staining is minimally affected in the mutant kidney. Scale bar = 100 μm. (Q) Quantitative RT-PCR of the E11.5 kidney. The columns represent means ± SD ($n = 3$). *$P < 0.05$, *R26Notch2* mice *versus* *Six2Cre/R26Notch2* mice.

Canonical Notch signals are mediated by the *Hes/Hesr* gene family members, which suppress the target genes.[22] Among the *Hes/Hesr* genes reported to be expressed in the metanephric mesenchyme,[23,24] *Hesr1* and *Hesr3* were dramatically upregulated under Notch2 activation, as shown by *in situ* hybridization at E12.5 (Figure 6, A–D). Although not detected by *in situ* hybridization at E11.5, RT-PCR analyses revealed increases in *Hesr1* and *Hesr3* at this stage, as well as an increase in the exogenous intracellular domain of *Notch2* (Figure 6, E and F), the latter of which is consistent with the activation timing of *Six2Cre* recombinase.[11] Although the *Hes1* and *Hes5* promoters in the developing kidney are driven by endogenous Notch activity,[25] we did not detect significant increases in these gene expressions under Notch2 activation (Figure 6E and data not shown). Therefore, we propose that *Notch2* activates *Hesr1/Hesr3*, which in turn could suppress *Pax2*, thereby leading to *Six2* reduction and ectopic *Wnt4* expression (Figure 6G). Alternatively, Hesr proteins may directly inhibit *Six2* expression.

DISCUSSION

We have shown that Notch2 activation results in depletion of *Six2*-positive nephron progenitors, which could arise through premature differentiation toward renal tubules via ectopic *Wnt4* activation. *Six2* reduction should be a key molecular event in producing these phenotypes, because *Six2Cre/R26Notch2* mice phe-

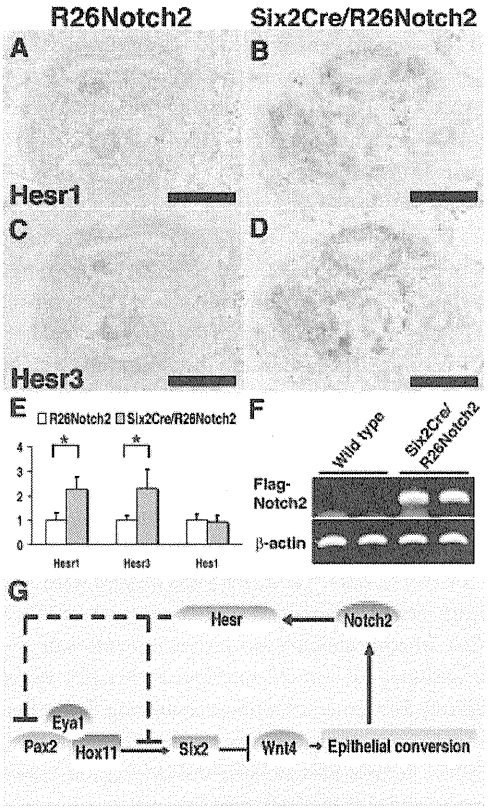

Figure 6. A Notch2-Wnt4-positive feedback loop stabilizes the differentiated state. (A and B) *In situ* hybridization of *Hesr1*. *Hesr1* expression is significantly increased in the *Six2Cre/R26Notch2* kidney at E12.5. (C and D) *In situ* hybridization of *Hesr3*. *Hesr3* expression is significantly increased in the *Six2Cre/R26Notch2* kidney at E12.5. Scale bar = 100 μm. (E) Quantitative RT-PCR of *Hesr1* and *Hesr3* in the E11.5 kidney. The columns represent means ± SD ($n = 3$). *$P < 0.05$, *R26Notch2* mice *versus* *Six2Cre/R26Notch2* mice. (F) RT-PCR of the exogenous intracellular domain of *Notch2* in E11.5 kidneys from wild-type mice ($n = 2$) and *Six2Cre/R26Notch2* mice ($n = 2$). (G) Proposed functions of Notch2 for the nephron progenitors. See the Discussion section for details.

nocopy *Six2*-deficient mice.[13] *Six2* expression is regulated by the Pax2/Eya1/Hox11 complex, and among these components, Pax2 was decreased under *Notch2* activation, which could reasonably explain the Six2 reduction. *Gdnf* is another direct target of the Pax2/Eya1/Hox11 complex, and the observed reduction in *Gdnf* expression under Notch2 activation further supports the decreased activity of the complex.

Canonical Notch signals are mediated by the Hes/Hesr family members, which suppress the target genes.[22] These family members either sequester positive basic helix-loop-helix transcription factors that bind to consensus sequences (E boxes) in the target promoters or actively repress the target genes by binding to different consensus sequences (N boxes or C sites) and recruiting the histone deacetylase (HDAC) complex. Among the family genes, *Hesr1* and *Hesr3* were upregulated under Notch2 activation. In addition, multiple potential N boxes and C sites exist in the proximal promoter of *Pax2* but not in that of *Hox11* (data not shown), and neither of these promoters contains E boxes. Therefore, we propose that Notch2 activates *Hesr1/Hesr3*, which could suppress *Pax2* possibly by recruiting the HDAC complex, which in turn leads to *Six2* reduction. Alternatively, Hesr proteins may directly inhibit Six2 expression, either by modulating the activity of the Pax2/Eya1/Hox11 complex or independently of the complex. It is also possible that the Notch2-mediated increase in Wnt4 secondarily affects the expression of Six2, although Hesr proteins are considered to be repressors, and Hesr-dependent Wnt4 activation has not been reported. To clarify these issues, it will be necessary to examine the binding sites of Hesr proteins and the possible interactions between Hesr proteins and the Pax2/Eya1/Hox11 complex, as well as to cross the activated Notch2 mice with Wnt4 or Hesr mutant mice.

Because *Notch2* deficiency results in the absence of the proximal nephrons, endogenous *Notch2* is critical for proximal nephron development, either by cell fate specification of the progenitors toward the proximal nephron or by stabilizing the proximal fate determined by other mechanisms. Although the former possibility is attractive, considering the lateral inhibition mechanisms of Notch in a variety of biologic processes, the latter is suggested because the initial proximodistal axis is still established under *Notch2* deficiency, which is likely to be mediated by Lim1-dependent mechanisms.[18,26] Our observations that *Notch2* activation did not lead to proximal fate specification further support this hypothesis. In the mutant mice, Notch2 activation was observed from E11.5 and was detected in all of the mesenchyme-derived epithelia at E14.5. Nonetheless, proximal tubules were not overrepresented. In contrast, *Notch1* deletion in the metanephric mesenchyme does not produce any specific phenotypes, whereas *Notch1* activation causes overproduction of proximal tubules and reductions in kidney size.[18] Cheng *et al.*[18] suggested that Notch1 may be a weaker activator of the target promoters of Notch2, possibly owing to differences in their tertiary structures, and that the level of endogenous Notch1 could be below the threshold required to activate Notch2 targets. In their experiments, *Notch1* was inserted into the *Rosa26* locus, and the same *Six2Cre* mouse strain was used. Therefore, our data indicate that even in the overexpressed state, Notch1 and Notch2 may emit overlapping yet different signals in the nephron progenitors. However, side-by-side comparisons are required to exclude any influences of the genetic background.

Nephrons are generated from the metanephric mesenchyme by successive activation of *Wnt4* and *Notch2*. *Wnt4* is required for the mesenchymal-to-epithelial transition, whereas *Notch2* plays a role in the development of the proximal nephron epithelia.[5,27] Our observation that Notch2 activation leads to *Wnt4* upregulation suggests the existence of a positive feedback loop (Figure 6G). Once Notch2 is activated, the feedback loop augments Wnt4 expression, which accelerates differentiation and inhibits reversion to the undifferentiated state. Therefore, we propose that Notch2 stabilizes, rather

than specifies, the nephron fate by shutting down the undifferentiated progenitor program once directed toward the differentiation pathway. It is important to note that Notch functions are highly context dependent. Although our data support a molecular model of dysregulated Notch2 in nephron progenitors, different mechanisms may apply to endogenous Notch2 signaling in cells that are committed to an epithelial fate. Notch2 overexpression in these nascent epithelial cells would address this point.

For regenerative medicine, it is desirable to be able to manipulate the cell fate specification of progenitors. However, our data suggest that premature Notch2 activation in the nephron progenitors does not serve this purpose. Instead, Notch2 signals could be used to stabilize the cell fate once specified. Therefore, the timing of Notch2 activation would be critical. Delayed activation of Notch2 by crossing *R26Notch2* mice with *Six2CreER* or *Wnt4Cre* mice would provide information for solving this problem, as well as augmenting our understanding of kidney development.[11] In addition, podocyte-specific Notch2 activation should be investigated, because Notch1 activation in this cell type leads to proteinuria and glomerulosclerosis.[28,29]

CONCISE METHODS

Gene Targeting and Generation of Mutant Mice

The *Notch2* fragment used for the experiment encompasses amino acids 1701 to 2470 and does not contain the transmembrane domain or S3 cleavage site but does contain the intact transactivation domain and C-terminal PEST sequences.[30] The Flag-tagged intracellular domain of *Notch2* was digested with *Sal*I and *Not*I and inserted into the *Sal*I-*Not*I sites of *pBigT*,[21] a vector containing an adenovirus splice acceptor sequence followed by a *PGK-neo* cassette and a tpA stop sequence flanked by two loxP sites. The resulting plasmid was digested with *Pac*I and *Asc*I to release the entire floxed neo-tpA and Notch2 assembly, which was inserted into the *Pac*I and *Asc*I sites of a modified *pRosa26-1* vector containing two homologous sequences to the *Rosa26* locus flanking the inserted sequence.[21] The resulting plasmid was linearized and used for electroporation. E14.1 ES cells (2×10^7) were electroporated with 50 μg of the targeting vector and allowed to grow on neomycin-resistant mouse embryonic fibroblasts in the presence of G418 (300 μg/ml). Successful targeting of 2 of 120 clones was confirmed by Southern blot analysis using genomic DNA digested with *Eco*RI. Primers (5′-AGG CGC CCG ATA GAA TAA AT-3′ and 5′-ACT CTT CCC CTC CCC CTA CT-3′) were used to generate a 607-bp 5′ probe (probe A; Figure 1A), which detected a 15.6-kb band for the wild-type sequence and a 4.3-kb band for the targeted sequence. Finally, the targeted ES clones were used to generate chimeric mice at the Center for Animal Resources and Development, Kumamoto University. All animal experiments were performed in accordance with institutional guidelines and ethics review committees.

Mouse Genotyping

Mice carrying the *R26Notch2* allele were genotyped with primers for Neo (forward primer Neo F, 5′-AAG GGA CTG GCT GCT ATT GG-3′ and reverse primer Neo R, 5′-ATA TCA CGG GTA GCC AAC GC-3′) and Rosa26 (forward primer Rosa26 F, 5′-GAG TTC TCT GCT GCC TCC TG-3′ and reverse primer Rosa26 R, 5′-CCG ACA AAA CCG AAA ATC TG-3′). Mice carrying the Cre allele were genotyped with forward primer Cre 1 (5′-AGG TTC GTT CAC TCA TGG A-3′) and reverse primer Cre 2 (5′-TCG ACC AGT TTA GTT ACC C-3′). PCR amplifications were performed under identical conditions using GoTaq DNA polymerase (Promega) with denaturation at 95°C for 5 minutes, followed by 35 cycles of 95°C for 30 seconds, 58°C for 60 seconds, and 72°C for 30 seconds, and a final extension at 72°C for 7 minutes. The PCR products were analyzed by electrophoresis in a 1.2% agarose gel and visualized by ethidium bromide staining.

In situ Hybridization and Immunostaining

Histologic examinations were performed as described previously.[9,31] Mice were fixed in 10% formalin, embedded in paraffin, and cut into 6-μm sections. *In situ* hybridization was performed using an automated Discovery System (Ventana) according to the manufacturer's protocols. The probes for *Wnt4*,[5] *Eya1*,[32] and *Hesr1* and *Hesr3*[33] were described in the cited papers. Templates for other probes were generated by RT-PCR and sequenced. Immunostaining was carried out automatically using a BlueMap or DABmap kit and the automated Discovery System (Ventana) or manually for immunofluorescence staining. The following primary antibodies were used: anti-Pax2 (Covance); anti-Six2;[34] anti-Sall1[35,36] (PPMX Perseus Proteomics); anti-cytokeratin (Sigma); anti-laminin (Sigma); and anti-DDDDK tag (Abcam).

Quantitative RT-PCR of the E11.5 Kidney

RNA was isolated from the dissected kidneys on both sides using an RNeasy Plus Micro Kit (Qiagen), and then reverse transcribed with random primers and Superscript III (Invitrogen). Quantitative PCR was carried out using a real-time PCR System (Applied Biosystems) and Thunderbird SYBR qPCR Mix (Toyobo). Two-step standard cycling conditions and sequence-specific primers were used (Supplementary Table 1). We analyzed the dissociation curves after each reaction to assess the specificity of the quantification. All of the samples were normalized by the β-actin expression using the relative standard curve method. We carried out three independent experiments, and representative data are shown.

ACKNOWLEDGMENTS

We thank A.P. McMahon for the *Six2Cre* mice; K. Hozumi, R. Kageyama, P.X. Xu, Y. Kawakami, and F. Costantini for plasmids; and K. Kawakami for the anti-Six2 antibody. We also thank N. Takeda, J. Nakai, Y. Tsurumoto, and T. Ohmori for technical assistance, and S.S. Tanaka and M. Ikeya for helpful discussions. This study was supported in part by Grants-in-Aid from the Ministry of Education, Culture, Sports, Science and Technology (MEXT) and by the Global COE Program (Cell Fate Regulation Research and Education Unit), MEXT, Japan.

DISCLOSURES

None.

REFERENCES

1. Moore MW, Klein RD, Farinas I, Sauer H, Armanini M, Phillips H, Reichardt LF, Ryan AM, Carver-Moore K, Rosenthal A: Renal and neuronal abnormalities in mice lacking GDNF. *Nature* 382: 76–79, 1996
2. Pichel JG, Shen L, Sheng HZ, Granholm AC, Drago J, Grinberg A, Lee EJ, Huang SP, Saarma M, Hoffer BJ, Sariola H, Westphal H: Defects in enteric innervation and kidney development in mice lacking GDNF. *Nature* 382: 73–76, 1996
3. Sanchez MP, Silos-Santiago I, Frisen J, He B, Lira SA, Barbacid M: Renal agenesis and the absence of enteric neurons in mice lacking GDNF. *Nature* 382: 70–73, 1996
4. Carroll TJ, Park JS, Hayashi S, Majumdar A, McMahon AP: Wnt9b plays a central role in the regulation of mesenchymal to epithelial transitions underlying organogenesis of the mammalian urogenital system. *Dev Cell* 9: 283–292, 2005
5. Stark K, Vainio S, Vassileva G, McMahon AP: Epithelial transformation of metanephric mesenchyme in the developing kidney regulated by Wnt-4. *Nature* 372: 679–683, 1994
6. Kispert A, Vainio S, McMahon AP: Wnt-4 is a mesenchymal signal for epithelial transformation of metanephric mesenchyme in the developing kidney. *Development* 125: 4225–4234, 1998
7. Herzlinger D, Koseki C, Mikawa T, al-Awqati Q: Metanephric mesenchyme contains multipotent stem cells whose fate is restricted after induction. *Development* 114: 565–572, 1992
8. Osafune K, Takasato M, Kispert A, Asashima M, Nishinakamura R: Identification of multipotent progenitors in the embryonic mouse kidney by a novel colony-forming assay. *Development* 133: 151–161, 2006
9. Nishinakamura R, Matsumoto Y, Nakao K, Nakamura K, Sato A, Copeland NG, Gilbert DJ, Jenkins NA, Scully S, Lacey DL, Katsuki M, Asashima M, Yokota T: Murine homolog of SALL1 is essential for ureteric bud invasion in kidney development. *Development* 128: 3105–3115, 2001
10. Nishinakamura R: Stem cells in the embryonic kidney. *Kidney Int* 73: 913–917, 2008
11. Kobayashi A, Valerius MT, Mugford JW, Carroll TJ, Self M, Oliver G, McMahon AP: Six2 defines and regulates a multipotent self-renewing nephron progenitor population throughout mammalian kidney development. *Cell Stem Cell* 3: 169–181, 2008
12. Takasato M, Osafune K, Matsumoto Y, Kataoka Y, Yoshida N, Meguro H, Aburatani H, Asashima M, Nishinakamura R: Identification of kidney mesenchymal genes by a combination of microarray analysis and Sall1-GFP knockin mice. *Mech Dev* 121: 547–557, 2004
13. Self M, Lagutin OV, Bowling B, Hendrix J, Cai Y, Dressler GR, Oliver G: Six2 is required for suppression of nephrogenesis and progenitor renewal in the developing kidney. *EMBO J* 25: 5214–5228, 2006
14. Gong KQ, Yallowitz AR, Sun H, Dressler GR, Wellik DM: A Hox-Eya-Pax complex regulates early kidney developmental gene expression. *Mol Cell Biol* 27: 7661–7668, 2007
15. Wellik DM, Hawkes PJ, Capecchi MR: Hox11 paralogous genes are essential for metanephric kidney induction. *Genes Dev* 16: 1423–1432, 2002
16. McCright B, Gao X, Shen L, Lozier J, Lan Y, Maguire M, Herzlinger D, Weinmaster G, Jiang R, Gridley T: Defects in development of the kidney, heart and eye vasculature in mice homozygous for a hypomorphic Notch2 mutation. *Development* 128: 491–502, 2001
17. Cheng HT, Miner JH, Lin M, Tansey MG, Roth K, Kopan R: Gamma-secretase activity is dispensable for mesenchyme-to-epithelium transition but required for podocyte and proximal tubule formation in developing mouse kidney. *Development* 130: 5031–5042, 2003
18. Cheng HT, Kim M, Valerius MT, Surendran K, Schuster-Gossler K, Gossler A, McMahon AP, Kopan R: Notch2, but not Notch1, is required for proximal fate acquisition in the mammalian nephron. *Development* 134: 801–811, 2007
19. McDaniell R, Warthen DM, Sanchez-Lara PA, Pai A, Krantz ID, Piccoli DA, Spinner NB: NOTCH2 mutations cause Alagille syndrome, a heterogeneous disorder of the notch signaling pathway. *Am J Hum Genet* 79: 169–173, 2006
20. Soriano P: Generalized lacZ expression with the ROSA26 Cre reporter strain. *Nat Genet* 21: 70–71, 1999
21. Srinivas S, Watanabe T, Lin CS, William CM, Tanabe Y, Jessell TM, Costantini F: Cre reporter strains produced by targeted insertion of EYFP and ECFP into the ROSA26 locus. *BMC Dev Biol* 1: 4, 2001
22. Kageyama R, Ohtsuka T, Kobayashi T: The Hes gene family: Repressors and oscillators that orchestrate embryogenesis. *Development* 134: 1243–1251, 2007
23. Piscione TD, Wu MY, Quaggin SE: Expression of Hairy/Enhancer of Split genes, Hes1 and Hes5, during murine nephron morphogenesis. *Gene Expr Patterns* 4: 707–711, 2004
24. Chen L, Al-Awqati Q: Segmental expression of Notch and Hairy genes in nephrogenesis. *Am J Physiol Renal Physiol* 288: F939–F952, 2005
25. Ong CT, Cheng HT, Chang LW, Ohtsuka T, Kageyama R, Stormo GD, Kopan R: Target selectivity of vertebrate notch proteins. Collaboration between discrete domains and CSL-binding site architecture determines activation probability. *J Biol Chem* 281: 5106–5119, 2006
26. Kobayashi A, Kwan KM, Carroll TJ, McMahon AP, Mendelsohn CL, Behringer RR: Distinct and sequential tissue-specific activities of the LIM-class homeobox gene Lim1 for tubular morphogenesis during kidney development. *Development* 132: 2809–2823, 2005
27. Kopan R, Cheng HT, Surendran K: Molecular insights into segmentation along the proximal-distal axis of the nephron. *J Am Soc Nephrol* 18: 2014–2020, 2007
28. Niranjan T, Bielesz B, Gruenwald A, Ponda MP, Kopp JB, Thomas DB, Susztak K: The Notch pathway in podocytes plays a role in the development of glomerular disease. *Nat Med* 14: 290–298, 2008
29. Waters AM, Wu MY, Onay T, Scutaru J, Liu J, Lobe CG, Quaggin SE, Piscione TD: Ectopic notch activation in developing podocytes causes glomerulosclerosis. *J Am Soc Nephrol* 19: 1139–1157, 2008
30. Hozumi K, Abe N, Chiba S, Hirai H, Habu S: Active form of Notch members can enforce T lymphopoiesis on lymphoid progenitors in the monolayer culture specific for B cell development. *J Immunol* 170: 4973–4979, 2003
31. Sakaki-Yumoto M, Kobayashi C, Sato A, Fujimura S, Matsumoto Y, Takasato M, Kodama T, Aburatani H, Asashima M, Yoshida N, Nishinakamura R: The murine homolog of SALL4, a causative gene in Okihiro syndrome, is essential for embryonic stem cell proliferation, and cooperates with Sall1 in anorectal, heart, brain and kidney development. *Development* 133: 3005–3013, 2006
32. Xu PX, Zheng W, Laclef C, Maire P, Maas RL, Peters H, Xu X: Eya1 is required for the morphogenesis of mammalian thymus, parathyroid and thyroid. *Development* 129: 3033–3044, 2002
33. Sakamoto M, Hirata H, Ohtsuka T, Bessho Y, Kageyama R: The basic helix-loop-helix genes Hesr1/Hey1 and Hesr2/Hey2 regulate maintenance of neural precursor cells in the brain. *J Biol Chem* 278: 44808–44815, 2003
34. Ohto H, Takizawa T, Saito T, Kobayashi M, Ikeda K, Kawakami K: Tissue and developmental distribution of Six family gene products. *Int J Dev Biol* 42: 141–148, 1998
35. Sato A, Kishida S, Tanaka T, Kikuchi A, Kodama T, Asashima M, Nishinakamura R: Sall1, a causative gene for Townes-Brocks syndrome, enhances the canonical Wnt signaling by localizing to heterochromatin. *Biochem Biophys Res Commun* 319: 103–113, 2004
36. Yuri S, Fujimura S, Nimura, Takeda N, Toyooka Y, Fujimura Y, Aburatani H, Ura K, Koseki H, Niwa H, Nishinakamura R: Sall4 is essential for stabilization, but not pluripotency, of embryonic stem cells by repressing aberrant trophectoderm gene expression. *Stem Cells* 27: 796–805, 2009

Kif26b, a kinesin family gene, regulates adhesion of the embryonic kidney mesenchyme

Yukako Uchiyama[a,b,1], Masaji Sakaguchi[a,b,c,1], Takeshi Terabayashi[a,b], Toshiaki Inenaga[a], Shuji Inoue[a,b], Chiyoko Kobayashi[a], Naoko Oshima[d], Hiroshi Kiyonari[d], Naomi Nakagata[e], Yuya Sato[f], Kiyotoshi Sekiguchi[f], Hiroaki Miki[g], Eiichi Araki[c], Sayoko Fujimura[a], Satomi S. Tanaka[a], and Ryuichi Nishinakamura[a,b,2]

[a]Department of Kidney Development, Institute of Molecular Embryology and Genetics, Kumamoto University, Kumamoto 860-0811, Japan; [b]Global COE "Cell Fate Regulation Research and Education Unit," Kumamoto University, Kumamoto 860-0811, Japan; [c]Department of Metabolic Medicine, Graduate School of Medical Sciences, Kumamoto University, Kumamoto 860-8556, Japan; [d]Laboratory for Animal Resources and Genetic Engineering, RIKEN Center for Developmental Biology, Kobe 650-0047, Japan; [e]Division of Reproductive Engineering, Center for Animal Resources and Development, Kumamoto University, Kumamoto 860-0811, Japan; [f]Laboratory of Extracellular Matrix Biochemistry, Institute for Protein Research, Osaka University, Osaka 565-0871, Japan; and [g]Laboratory of Intracellular Signaling, Institute for Protein Research, Osaka University, Osaka 565-0871, Japan

Edited by Eric N. Olson, University of Texas Southwestern, Dallas, TX, and approved April 15, 2010 (received for review November 27, 2009)

The kidney develops through reciprocal interactions between two precursor tissues: the metanephric mesenchyme and the ureteric bud. We previously demonstrated that the zinc finger protein Sall1 is essential for ureteric bud attraction toward the mesenchyme. Here, we show that *Kif26b*, a kinesin family gene, is a downstream target of *Sall1* and that disruption of this gene causes kidney agenesis because of impaired ureteric bud attraction. In the *Kif26b*-null metanephros, compact adhesion between mesenchymal cells adjacent to the ureteric buds and the polarized distribution of integrin α8 were impaired, resulting in failed maintenance of *Gdnf*, a critical ureteric bud attractant. Overexpression of Kif26b in vitro caused increased cell adhesion through interactions with nonmuscle myosin. Thus, Kif26b is essential for kidney development because it regulates the adhesion of mesenchymal cells in contact with ureteric buds.

kinesin | Gdnf | kidney development | metanephric mesenchyme | Sall1

In the developing kidney, the metanephric mesenchyme secretes glial cell line-derived neurotrophic factor (GDNF), which induces the budding of ureteric buds from the Wolffian duct. Upon contact with ureteric buds, adjacent metanephric mesenchymal cells condense around the tips of the ureteric buds. Concomitantly, integrin α8 expressed in the mesenchyme is polarized on the cell surface facing the ureteric buds. Integrin α8 interacts with its ligand nephronectin expressed on the surface of the ureteric bud epithelia. This interaction is essential for the maintenance, but not the initiation, of *Gdnf* expression in the mesenchyme and for further attraction of ureteric buds, although the precise mechanisms remain unknown. Thus, genetic ablation of nephronectin or integrin α8 results in the failure of *Gdnf* maintenance and kidney agenesis (1, 2). Subsequently, Wnt9b secreted from the ureteric buds induces Wnt4 expression in the mesenchyme (3). Wnt4 functions in a cell-autonomous manner to transform the mesenchyme to epithelia, which differentiate into each segment of nephrons, including the glomerulus, proximal tubule, Henle's loop, and distal tubule (4). This Wnt4-mediated differentiation is antagonized by the transcription factor Six2 that functions to maintain nephron progenitors (5, 6).

We previously reported that the nuclear zinc-finger protein Sall1 is essential for ureteric bud attraction in kidney development and that metanephric mesenchymal cells that highly express Sall1 contain multipotent nephron progenitors (7, 8). To examine the molecular pathways regulated by Sall1, we searched for genes that are predominantly expressed in Sall1-positive mesenchymal cells by cDNA microarray analysis using *Sall1-GFP* knock-in mice (9). Here, we describe that *Kif26b*, a kinesin family gene, acts downstream of *Sall1* and regulates the adhesion of mesenchymal cells surrounding ureteric buds, providing insights into the mechanisms of kidney development.

Results

Kif26b Is Expressed in the Metanephric Mesenchyme During Nephrogenesis. Mouse full-length *Kif26b* encodes a 2,112-aa protein that shows 87% amino acid homology with human *KIF26B* and has a well conserved motor domain (96% identical to human *KIF26B*) in the N terminus (GenBank accession no. AB355846). Kinesins constitute a large family of intracellular motor proteins, some of which transport cargos along microtubules. Forty-five members have so far been identified in mice and humans, and are involved in many processes such as organelle transport, intraflagellar transport, and cell signaling (10). The functions of *Kif26b*, which is classified into the kinesin-11 family, remain unknown (11).

We first examined *Kif26b* expression in the embryonic kidney by in situ hybridization. *Kif26b* was detected in the metanephric mesenchyme at embryonic day (E) 10.5 (Fig. 1*A*). After E11.5, its expression was observed in mesenchymal cells surrounding the tips of ureteric buds in the metanephroi (Fig. 1 *B* and *C*). At E14.5, *Kif26b* was strongly expressed in the nephrogenic zone (Fig. 1*D*, arrowheads) where the nephron progenitor marker *Six2* was also detected (Fig. 1*E*). Notably, among the *Sall1*-positive domains, *Kif26b* signals were only present in the uncommitted mesenchyme and absent from more differentiated structures including renal vesicles and comma-shaped bodies (Fig. 1*F*, arrow). Immunostaining showed that Kif26b protein was localized in the cytosol of mesenchymal cells (Fig. 1*G*). Furthermore, the expression of Kif26b was markedly reduced in *Sall1*-null metanephroi, suggesting that *Kif26b* is a genetic downstream target of *Sall1* in the metanephric mesenchyme (Fig. 1 *H* and *I*, and Fig. S1*A*). Indeed, multiple Sall1-binding consensus sequences were found in the *Kif26b* promoter (12), and a biotinylated oligonucleotide probe of this region, but not a mutated one, precipitated endogenous Sall1 protein in newborn kidney lysates (Fig. 1*J* and Fig. S1*B*). Chromatin immunoprecipitation (ChIP) using an anti-Sall1 antibody also confirmed Sall1 binding to the *Kif26b* promoter (Fig. 1*K*). Furthermore, overexpression of Sall1 enhanced

Author contributions: Y.U., M.S., and R.N. designed research; Y.U., M.S., T.T., T.I., S.I., C.K., S.F., and R.N. performed research; N.O., H.K., N.N., Y.S., and K.S. contributed new reagents/analytic tools; Y.U., M.S., T.T., T.I., K.S., H.M., E.A., S.S.T., and R.N. analyzed data; and Y.U. and R.N. wrote the paper.

The authors declare no conflict of interest.

This article is a PNAS Direct Submission.

Data deposition: The sequence reported in this paper has been deposited in the DNA Data Bank of Japan/European Molecular Biology Laboratory/GenBank databases (accession no. AB355846).

[1]Y.U. and M.S. contributed equally to this work.

[2]To whom correspondence should be addressed. E-mail: ryuichi@gpo.kumamoto-u.ac.jp.

This article contains supporting information online at www.pnas.org/lookup/suppl/doi:10.1073/pnas.0913748107/-/DCSupplemental.

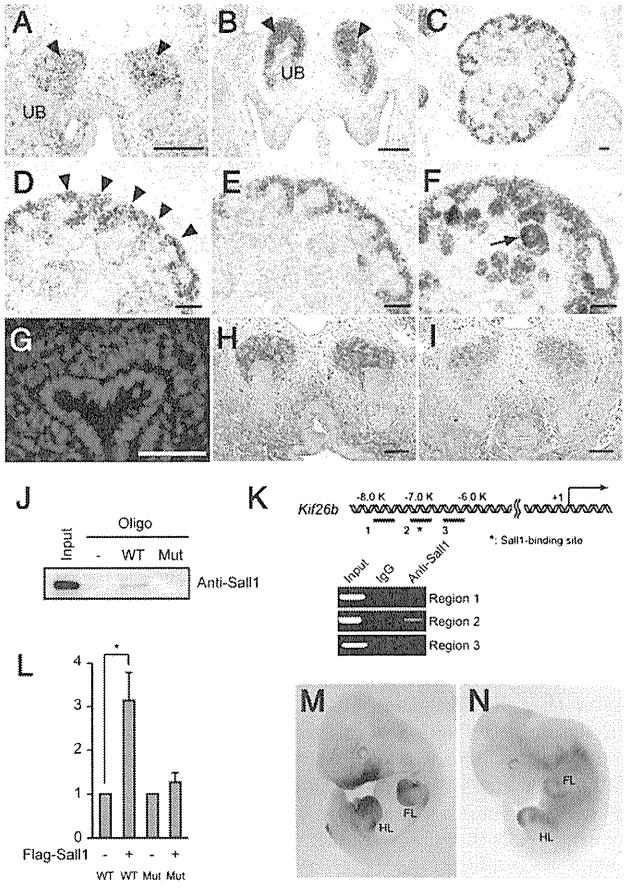

Fig. 1. Expression of Kif26b in the metanephric mesenchyme. (*A–F*) Transverse sections through the metanephric regions of mouse embryos at E10.5 (*A*), E11.5 (*B*), and E14.5 (*C–F*) stained by in situ hybridization for *Kif26b* (*A–D*), *Six2* (*E*), and *Sall1* (*F*). Arrowheads, mesenchymal cells; arrow, comma-shaped body; UB, ureteric bud. (Scale bars, 100 μm.) (*G*) Cytosolic localization of endogenous Kif26b protein. Sections of embryonic kidneys at E11.5 were immunostained with an anti-Kif26b antibody (red). Nuclei were visualized by DAPI staining. (Scale bar, 100 μm.) (*H* and *I*) Reduced Kif26b expression in the *Sall1*-null mesenchyme (*I*) at E11.5 compared with the wild-type mesenchyme (*H*), as evaluated by immunostaining for Kif26b. (Scale bars, 100 μm.) (*J*) Binding of endogenous Sall1 protein to the promoter sequences of *Kif26b*. Newborn kidney lysates were incubated with a biotinylated oligonucleotide probe, pulled down with streptavidin beads, and immunoblotted with an anti-Sall1 antibody. (*K*) ChIP analysis using embryonic kidney lysates and the anti-Sall1 antibody. The pulled down DNA was amplified for the *Kif26b* promoter sequences. (*L*) Activation of the *Kif26b* promoter activity by Sall1. (M) *Kif26b* expression in the limb buds and central nervous system, as evaluated by whole-mount in situ hybridization of *Kif26b* at E11.5. FL, forelimb; HL, hindlimb. (*N*) Whole-mount X-gal staining of a *Kif26b-lacZ* mouse at E11.5.

the activity of a luciferase construct fused to the *Kif26b* promoter (Fig. 1*L*). Thus, *Kif26b* is expressed in the metanephric mesenchyme and is a direct downstream target of *Sall1*. *Kif26b* was also detected in other parts of the embryos such as the limb buds and central nervous system (Fig. 1 *M* and *N*).

Kif26b Ablation Causes Kidney Agenesis Owing to Impaired Ureteric Bud Invasion into the Metanephric Mesenchyme. To examine whether *Kif26b* has a functional role in kidney development, we used gene targeting to generate *Kif26b*-deficient mice (Fig. S2). Heterozygous mice were viable and fertile, and offspring were born at the expected Mendelian frequency. However, *Kif26b*$^{-/-}$ mice died within 24 h after birth. At birth, 22 of 33 (66.7%) mutant mice showed bilateral kidney agenesis, 9 (27.3%) showed unilateral kidney agenesis and hypoplasia on the other side, and 2 (6.0%) had bilateral small kidneys (Fig. 2*A*). The remaining kidneys were significantly reduced in size, and the mesenchyme in the cortical nephrogenic zone had almost disappeared (Fig. 2*B*). The development of other organs was apparently normal. Although *Kif26b*-null kidneys showed no histological differences from wild-type kidneys until E10.5 (Fig. 2 *C* and *D*), ureteric bud attraction was impaired after E11.0 (Fig. 2 *E* and *F*). In the mutant embryos, the ureteric buds were attracted close to the mesenchyme but failed to invade and branch into the mesenchyme (Fig. 2 *G* to *J*), and the kidney disappeared by E14.5 (Fig. 2 *K* and *L*). The mesenchymal cells underwent apoptotic cell death at E12.5, as shown by cleaved caspase-3 staining (Fig. 2 *M* and *N*). Bilateral ureteric attraction failure was observed in 7 of 11 (63.6%) mutant embryos at E11.0–11.5, while the remaining mutant embryos showed invasion of the ureteric bud on one side (2 of 11, 18.2%) or both sides (2 of 11, 18.2%), although to lesser extents compared with the wild-type embryos. These frequencies were fairly well correlated with those of the renal abnormalities in the newborn mice. Therefore, *Kif26b* is essential for ureteric bud attraction and could be one of the major functional molecules

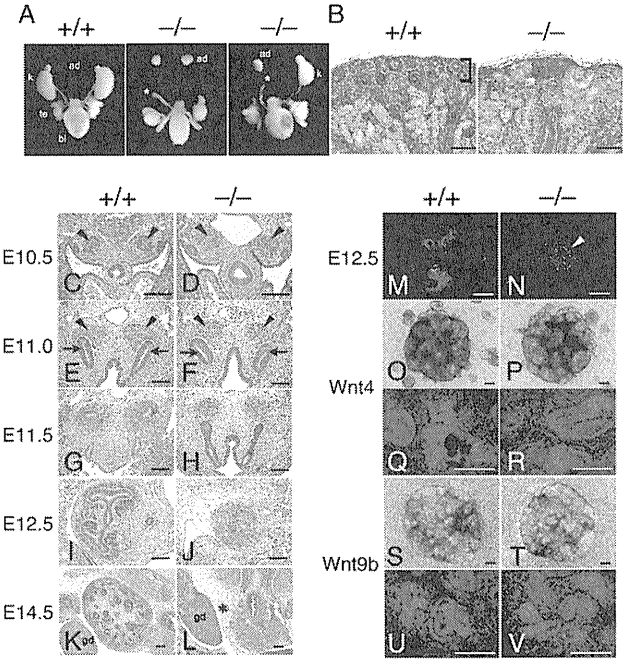

Fig. 2. Kidney agenesis and impaired ureteric bud attraction in *Kif26b*-null mutants. (*A*) Urogenital tissues from wild-type (*Left*) and *Kif26b*-null (*Center* and *Right*) newborn mice. ad, adrenal gland; k, kidney; te, testis; bl, bladder. Asterisk, blind-ended ureter. (*B*) Hematoxylin and eosin staining of a wild-type kidney and a mutant remnant kidney in newborn mice. Square bracket, mesenchyme in the cortical nephrogenic zone. (Scale bars, 100 μm.) (*C–L*) Failure of ureteric bud attraction under *Kif26b* deficiency. Wild-type and *Kif26b*-null embryonic kidneys were stained with hematoxylin and eosin. Arrowheads, metanephric mesenchyme; arrows, ureteric buds; gd, gonad; asterisk, remnant kidney. (*M* and *N*) Cleaved caspase-3-positive cells (arrowhead) in the Sall1-positive mesenchyme in *Kif26b*-null embryos at E12.5. Sections were immunostained for Sall1 (red) and cleaved caspase-3 (green). (Scale bars, 100 μm.) (*O–R*) Intact potency for epithelial conversion of the *Kif26b*-null mesenchyme. Metanephric mesenchyme was cultured on 3T3 cells expressing Wnt4. The samples shown in *Q* and *R* were stained with an anti-E-cadherin antibody and DAPI. (Scale bars, 100 μm.) (*S–V*) Metanephric mesenchyme was cultured on L-cells expressing Wnt9. The samples shown in *U* and *V* were stained with an anti-E-cadherin antibody and DAPI. (Scale bars, 100 μm.)

acting downstream of *Sall1*, because *Sall1*-null mice also show impaired ureteric bud attraction (7).

To examine whether the developmental potency of the mesenchyme after ureteric bud attraction was impaired in the absence of *Kif26b*, the mutant mesenchyme was separated from the ureteric buds and cultured on 3T3 feeder cells expressing Wnt4, a potent inducer of the mesenchyme-to-epithelial transition (13, 14). Almost all of the wild-type (11 of 11) (Fig. 2*O*) and mutant (6 of 7) (Fig. 2*P*) mesenchymes formed tubular structures within 3 days, and epithelial conversion was confirmed by E-cadherin staining (Fig. 2 *Q* and *R*). Because Wnt9b is an initial inducer secreted from the ureteric buds (3), we also confirmed the mesenchyme-to-epithelial transition in wild-type (5 of 5) and mutant (4 of 4) mesenchymes using feeder cells expressing Wnt9b (Fig. 2 *S–V*). Thus, the *Kif26b*-deficient mesenchyme retains its potency for epithelial conversion, but the failure of ureteric bud attraction probably causes subsequent defects in kidney development.

Kif26b Is Essential for the Maintenance of GDNF. GDNF is a major ureteric bud attractant. *Gdnf* was not properly maintained in the *Kif26b*-null mesenchyme at E11.5 (Fig. 3*A*), although its initial expression was intact until E10.75 (Fig. 3*B*). Phosphorylation of ERK and expression of *Wnt11*, which are both induced in ureteric tips by GDNF signaling (15), were also reduced (Fig. 3*A*). In contrast, Wnt9b was still expressed in the ureteric bud stalks (Fig. 3*A*). The *Gdnf* reduction was not caused by loss of mesenchymal cells, because we did not observe increased apoptosis evaluated by cleaved caspase-3 staining (Fig. S3*A*). Moreover, *Kif26b*$^{+/-}$*Gdnf*$^{+/-}$ mice showed more severe kidney phenotypes than *Kif26b*$^{+/-}$ or *Gdnf*$^{+/-}$ mice (Table 1), indicating there was a genetic link between *Kif26b* and the *Gdnf* pathway. Therefore, failure of *Gdnf* maintenance in the mutant embryos is likely to explain the phenotypic abnormalities in the ureteric bud attraction.

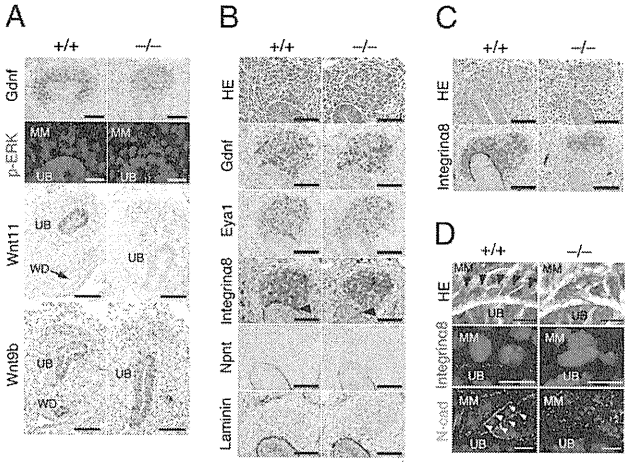

Fig. 3. Impaired condensation and *Gdnf* maintenance in the *Kif26b*-null mesenchyme. (*A*) Reduced expression of *Gdnf* and downstream signaling events in *Kif26b* mutant embryos at E11.5. Sections at E11.5 were stained by in situ hybridization for *Gdnf* and *Wnt11*, or immunostained for p-ERK (red) and pan-cytokeratin (green). Wnt9b is still expressed in the ureteric bud stalks. MM, metanephric mesenchyme; UB, ureteric bud; WD, Wolffian duct. (Black scale bars, 100 μm; white scale bars, 20 μm.) (*B* and *C*) Altered integrin α8 localization in the *Kif26b*-null metanephric mesenchyme. Sections at E10.75 (*B*) or E11.0 (*C*) were stained with hematoxylin and eosin, stained by in situ hybridization for *Gdnf* and *Eya1*, or immunostained for integrin α8, nephronectin (Npnt), and laminin. Integrin α8 is detected at the interface between the mesenchyme and the ureteric bud (arrowhead) in the wild-type embryos, but not in the mutant embryos. Integrin α8 is also reduced in the mutant mesenchyme adjacent to the ureteric buds. (Scale bars, 100 μm.) (*D*) Impaired condensation of the *Kif26b*-null mesenchyme at E10.75. Sections were stained with hematoxylin and eosin or immunostained for integrin α8 (red) or N-cadherin (green) for metanephric regions. Black arrowheads, columnar mesenchymal cells adjacent to ureteric buds; white arrowheads, lateral expression of N-cadherin in condensed mesenchymal cells. Nuclei were visualized by DAPI staining. (Scale bars, 10 μm.)

Kif26b Is Essential for the Adhesion and Polarization of Mesenchymal Cells Surrounding Ureteric Buds. *Gdnf* initiation is regulated by several transcription factors such as Pax2 and Eya1, while *Gdnf* is maintained by interactions between the mesenchyme and the ureteric buds including the integrin α8-mediated pathway (2). Indeed, Pax2 and *Eya1* were expressed in the mutant metanephric mesenchyme (Fig. 3*B* and Fig. S3*B*). In contrast, integrin α8 expression in mesenchymal cells adjacent to ureteric buds, as well as that clearly detected at the interface between the mesenchyme and the ureteric buds in wild-type embryos, was not observed in the mutant embryos at E10.75 when *Gdnf* was still expressed (Fig. 3*B*). Reduced integrin α8 expression in the mutant mesenchyme was more apparent at E11.0 (Fig. 3*C*). The integrin α8 ligand nephronectin and a basement protein laminin displayed no obvious differences between wild-type and mutant embryos (Fig. 3*B*). Double-staining for Sall1 and integrin α8 also confirmed that integrin α8 was reduced at the ureteric bud/mesenchyme junction when the mesenchyme was in contact with the ureteric bud (Fig. S3*C*). Therefore, integrin α8 reduction is unlikely to be secondary to the lack of ureteric bud invasion. The reduced ERK phosphorylation observed in the mutant mesenchyme (Fig. 3*A*) could imply impaired integrin signaling in this population. A reduction of integrin α8 in the mesenchyme close to the ureteric buds was also observed in *Kif26b* mutant embryos with milder phenotypes, in which the ureteric buds invaded into the mesenchyme to some extent (Fig. S3*D*). Thus, mutant mesenchymal cells that make contact with the ureteric bud tips were unable to establish the polarized localization of integrin α8, which probably led to the failure of *Gdnf* maintenance.

The mesenchymal cells adjacent to the ureteric buds were tightly cohered laterally and exhibited columnar alignment in the wild-type embryo, representing the initial histological indication of an interaction between the mesenchyme and the ureteric buds (Fig. 3*D*, black arrowheads). These mesenchymal cells showed a polarized distribution of integrin α8 on the basal side facing the ureteric buds (Fig. 3*D*). Basolateral N-cadherin staining also revealed that there was a strip of mesenchymal cells that exhibited columnar shapes along the ureteric bud tips in the wild-type embryo (Fig. 3*D*, white arrowheads). However, this condensation was not apparent in *Kif26b*-null mesenchymal cells adjacent to the ureteric bud tips (Fig. 3*D*). Therefore, mesenchymal cells that directly contact the ureteric buds could lose their basolateral integrity in the absence of *Kif26b*.

Similar abnormalities, including impaired integrin α8 and N-cadherin staining, were observed in the *Sall1*-deficient mesenchyme (Fig. S1*C*). Therefore, Kif26b could play a major functional role downstream of Sall1.

Table 1. Exacerbation of kidney phenotypes in compound mutant mice for *Kif26b* and *Gdnf*

Genotype	Kidney phenotypes			
	Normal	Hypoplasia	Agenesis	Total
Kif$^{+/-}$	50 (100)	0 (0)	0 (0)	50 (100)
Gdnf$^{+/-}$	39 (75.0)	4 (7.7)	9 (17.3)	52 (100)
Kif$^{+/-}$*Gdnf*$^{+/-}$	24 (46.2)	15 (28.8)*	13 (25.0)	52 (100)

The kidney phenotypes were analyzed at postnatal day 0. The data represent the number (percentage).
*$P < 0.01$, *Kif*$^{+/-}$*Gdnf*$^{+/-}$ mice vs. *Gdnf*$^{+/-}$ mice by the χ^2 test.

Kif26b Affects Cell Adhesion via an Interaction with Nonmuscle Myosin Heavy Chain II. To more closely study the role of Kif26b in the morphological changes of mesenchymal cells, we generated three independent human embryonic kidney (HEK) 293 cell lines overexpressing Flag-tagged Kif26b in a tetracycline-dependent manner. Each clone aggregated dramatically within 24 h in the presence of tetracycline (Fig. 4*A* and Fig. S4*A*). The cells showed enhanced calcium-dependent cell–cell adhesion, as assessed by dissociation assays (Fig. 4*B*). Indeed, knockdown of N-cadherin by a siRNA reduced the aggregation of Kif26b-overexpressing cells (Fig. 4*C* and Fig. S4 *C* and *D*). There were no significant changes in the expression levels of *Gdnf* and other transcription factors related to kidney development (Fig. S5*A*). The GDNF concentration was not increased in the supernatants (Fig. S5*B*). Thus, N-cadherin-dependent cell–cell adhesion is likely to be a primary event caused by Kif26b.

Many Kif proteins containing N-terminal motor domains interact with other molecules through their C-terminal regions (10). Indeed, cell aggregation was not observed when Kif26b lacking the C-terminal region (Kif26bΔC) was overexpressed in a tetracycline-dependent manner (Fig. 4*A*). The induction of the truncated proteins was more robust than that of the full-length protein, but the cells still exhibited no morphological changes (Fig. S4 *A* and *B*). Thus, we performed a pull-down assay using the GST-tagged C-terminal region of Kif26b, followed by mass spectrometry (Fig. 4*D*). Among the candidates, nonmuscle myosin heavy chain type IIB (NMHC IIB; MYH10) was confirmed as an interacting protein by coimmunoprecipitation experiments (Fig. 4*E*). Immunoprecipitation of MYH10 with deletion con-

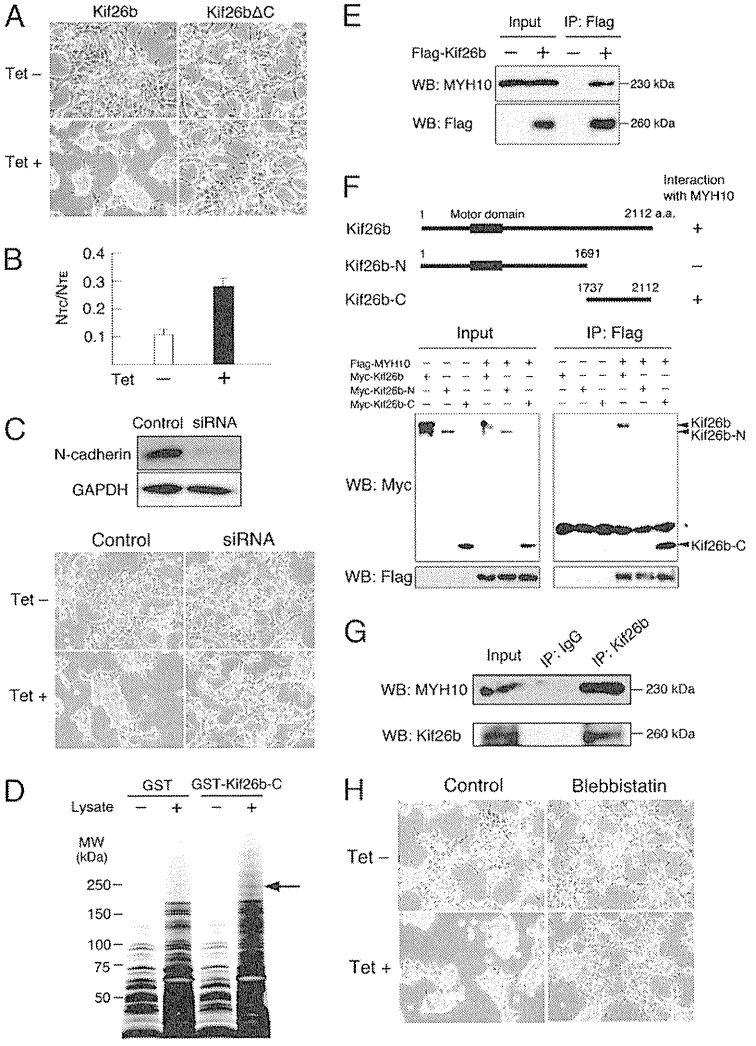

Fig. 4. Enhanced aggregation and cell adhesion by Kif26b overexpression. (*A*) Increased cell aggregation by Flag-tagged Kif26b overexpression. HEK293 cells were cultured for 48 h with or without tetracycline. No morphological changes are observed after overexpression of Kif26b lacking a C-terminal region (Kif26bΔC). (*B*) Increased calcium-dependent cell adhesion after Kif26b overexpression. Cells were incubated with (TC treatment) or without (TE treatment) calcium. Dissociation of the cells is represented by the index N_{TC}/N_{TE}, where N_{TC} and N_{TE} are the numbers of cell clusters after the TC and TE treatments, respectively. (*C*) Reduced aggregation by N-cadherin knockdown with a siRNA. Knockdown of N-cadherin was confirmed by immunoblotting. (*D*) GST pull-down complexes were analyzed by SDS/PAGE and silver staining. The arrow indicates the band for MYH10. (*E*) Interaction of Kif26b and MYH10. Immunoprecipitation was performed using HEK293 cells expressing tetracycline-inducible Flag-tagged Kif26b. (*F*) Deletion constructs of Kif26b and interaction of the C-terminal region of Kif26b and MYH10. Flag-MYH10 is coprecipitated with myc-tagged Kif26b. (*G*) Interaction of endogenous Kif26b and MYH10. MYH10 is coprecipitated with Kif26b from newborn mouse kidney lysates. (*H*) Effect of the NMHC II inhibitor blebbistatin on cell aggregation induced by tetracycline. Microscopic images of HEK293 cells incubated with and without tetracycline and blebbistatin for 24 h are shown.

structs of Kif26b also confirmed the specific interaction of the C-terminal region of Kif26b and MYH10 (Fig. 4*F*). The endogenous association of Kif26b and MYH10 was further confirmed using newborn kidney lysates (Fig. 4*G* and Fig. S6*A*). MYH10 was not only expressed in the mesenchyme but also in the ureteric buds, whereas Kif26b expression was specific to the mesenchyme (Fig. S6*B*), indicating an overlap of the expression domains of these two proteins. Furthermore, a specific NMHC II inhibitor, blebbistatin, inhibited the effect of Kif26b-dependent cell aggregation (Fig. 4*H*). These results suggest that Kif26b could regulate cell adhesion by interacting with NMHC II. Because accumulating evidence suggests that NMHC II augments cell adhesion by regulating actin filaments and cadherins (16), we propose that Kif26b may enhance the interaction of NMHC II and actin, thereby stabilizing the cell–cell adhesion of mesenchymal cells in the developing kidney.

Kif26b Is Not Required for the Function of Cilia. Finally, because another kinesin protein, Kif3, is involved in the transport of cilia components in the embryonic kidney, we examined the effect of Kif26b on cilia (17, 18). Impairment of cilia formation in renal tubules leads to polycystic kidney diseases (19). Cilia also play important roles in signaling pathways including Shh (20), which is required for kidney development (21). However, when we overexpressed Kif26b in MDCK cells that had well developed cilia on their surface, Kif26b was localized in the cytosol, and not in the cilia (Fig. S7*A*). Cilia were also detected in the metanephric mesenchyme in both wild-type and *Kif26b*-deficient mice (Fig. S7*B*). Furthermore, when we genetically reduced the *Kif26b* alleles from heterozygous mice for *Shh* or its downstream effecter *Gli3*, the mice displayed no renal phenotypes (Fig. S7*C*). Therefore, *Kif26b* is unlikely to be involved in either cilia formation or Shh signaling.

Discussion

We have shown that *Kif26b*, a kinesin family gene, is essential for embryonic kidney development. Kif26b plays an important role in the compact adhesion between mesenchymal cells adjacent to the ureteric buds, possibly by interacting with nonmuscle myosin. This could lead to the establishment of the basolateral integrity of the mesenchyme and the polarized expression of integrin α8, which maintains the Gdnf expression required for further ureteric bud attraction.

Recently, it was reported that another kinesin-11 member, Kif26a, negatively regulates Gdnf-Ret signaling by binding to Grb2 in Ret-expressing enteric neurons (22). However, Kif26a is not expressed in the developing kidney. In addition, Kif26b is expressed in the Gdnf-expressing kidney mesenchyme, but not in Ret-expressing ureteric buds, and eventually exerts positive effects on Gdnf expression. Therefore, the molecular mechanism of Kif26b is distinct from that of Kif26a.

NMHC II plays an important role in cell adhesion because it provides tension for actin filaments, and this is required for the proper localization of cell adhesion proteins such as cadherins (16). *MYH9*-deficient embryonic stem cells and mouse embryos exhibit a loss of cell–cell adhesion (23), while *MYH10*-null mice show hydrocephalus caused by loss of cell–cell adhesion in the cells lining the spinal canal (24). In addition, Smy1p, a kinesin-11 member in *Saccharomyces cerevisiae*, induces a conformational change in the class V myosin Myo2p, which enhances its interaction with actin and causes cell protrusion in one direction (25, 26). Moreover, NMHC II-actin complexes appear to facilitate cross-talk between N-cadherin and integrins during cardiac development (27, 28). Therefore, we speculate that Kif26b may enhance the interaction of NMHC II and actin, thereby stabilizing the cell–cell adhesion of mesenchymal cells and the interaction between the mesenchyme and ureteric buds through integrins in the developing kidney.

It is known that Kif3 regulates N-cadherin expression on the cell surface by associating with KAP3, and that *KAP3*-deficient embryonic fibroblasts show impaired N-cadherin expression (29). However, Kif26b was not detected in fibroblasts. Therefore, Kif26b is unlikely to ubiquitously regulate N-cadherin transport.

To the best of our knowledge, this is the first report that a kinesin deficiency can cause the lack of an entire organ. Better understanding of the kinesin-mediated regulation in the kidney primordia will provide unique insights into organ development.

Experimental Procedures

Cloning of *Kif26b*. A 5.5-kb cDNA was obtained from the Mammalian Gene Collection (National Institute of Health) but lacked a 5′ portion as judged by a sequence comparison with the human *KIF26B* cDNA. We found another cDNA in the mouse database that showed homology to the 5′ portion of the human *KIF26B* cDNA and the 5′ region of the mouse *Kif26b* genome. RT-PCR using mouse embryos (E13.5) showed that the combined cDNA existed in vivo. The amplified fragments were sequenced and a comparison between the resultant cDNA and the mouse genome revealed an exon/intron structure of *Kif26b* that was compatible with that of human *KIF26B*.

Generation of *Kif26b*-Deficient Mice. A *Kif26b*-targeting vector was constructed by incorporating the 5′ 7.8-kb *Kif26b* genomic and 3′ 4.4-kb *Kif26b* fragments. Both fragments were amplified by PCR using LA Taq (Takara) into a vector that contained the β-galactosidase gene (*lacZ*), the neomycin resistance (*Neo*^{r}) gene (*PGK-Neo*), and the diphtheria toxin A subunit (pMC1DTA) in tandem (30) (details of the vector are available from www.cdb.riken.go.jp/arg/cassette.html). The targeting vector was electroporated into TT2 ES cells, and 3 of 192 G418-resistant clones were correctly targeted, as determined by PCR and Southern blotting analyses using 5′ or 3′ probes after XmnI or AseI digestion, respectively. Two ES clones were used to generate germline chimeras that were bred with C57BL/6J female mice. Mice homozygous for the *Kif26b*-targeted allele (accession no. CDB0440K; www.cdb.riken.jp/arg/mutant%20mice%20list.html) were obtained by intercrossing heterozygous mice. Even when *Neo*^{r} was deleted by crossing the *Kif26b* mutant mice with mice expressing Flp, the phenotypes and lacZ expression patterns were identical to those of the original mutant mice. Genotyping of the offspring was performed by PCR using a forward primer, 5′-CCATCACATGCAGAAGGCTA-3′, and two reverse primers, 5′-AGCATCGAAGGCAAACATCT-3′ and 5′-CCGTAATGGGATAGGTCACG-3′, producing products of 300 bp for the wild-type allele and 500 bp for the mutant allele. Northern blotting was performed using 4 mg of poly(A)+ RNA from E11.5 embryos per lane. Either a 5′ SalI-BamHI 1.25-kb fragment or a 3′ SphI-NheI 1.5-kb fragment was used as a probe.

In Situ Hybridization and Immunohistochemistry. Samples were fixed in 10% formalin and processed for paraffin-embedded sectioning. In situ hybridization and immunostaining were performed using an automated Discovery System (Ventana) according to the manufacturer's protocols (31). A 5′ 1.2-kb SalI-BamHI fragment or a 3′ 639-bp PCR-amplified fragment of the *Kif26b* cDNA was subcloned, and transcripts were generated with T7 RNA polymerase and DIG-RNA labeling mix (Roche). Both probes showed similar expression patterns. Other probes were isolated by PCR or were described previously (32).

For fluorescence immunohistochemistry, paraffin-embedded sections were deparaffinized and autoclaved at 121 °C for 5 min in citrate buffer (pH 6.0). After incubation in blocking solution for 1 h at room temperature, the sections were incubated overnight with primary antibodies at 4 °C, followed by incubation with secondary antibodies conjugated with Alexa Fluor 488 or 594 (Invitrogen). For whole-mount staining, metanephric explants were fixed with 4% paraformaldehyde, blocked with 1% BSA, and incubated overnight with primary antibodies at 4 °C, followed by incubation with secondary antibodies. The primary antibodies used were: anti-Sall1 (31) (Perseus Proteomics); anti-cleaved caspase-3 (Cell Signaling); anti-pan-cytokeratin (Sigma); anti-E-cadherin (BD Transduction Laboratories); anti-phosphorylated Erk (Cell Signaling); anti-α8 integrin (1); anti-N-cadherin (Santa Cruz Biotechnology); anti-MYH10 (Cell Signaling or Developmental Studies Hybridoma Bank); and anti-acetylated α-tubulin (Sigma). A polyclonal antibody against mouse nephronectin was produced by immunizing rabbits with FLAG-tagged recombinant mouse nephronectin (33). The antibody was purified by affinity chromatography using columns of 6× His-tagged mouse nephronectin immobilized on CNBr-activated Sepharose 4B (GE Healthcare). We generated a polyclonal anti-Kif26b antibody by immunizing rabbits with GST-fused Kif26 protein (amino acids 1402–2112). The specificity of the anti-Kif26b antibody was confirmed using *Kfi26b*-null kidney sections.

GST Pull-Down Assay and Mass Spectrometry. The C-terminal *Kif26b* fragment corresponding to amino acids 1737–2112 was cloned into *pGEX6P-1* (GE Healthcare) and introduced into BL21 (DE3). GST-fused Kif26b protein bound to Glutathione-Sepharose 4B beads (GE Healthcare) was incubated with newborn kidney or brain samples lysed in buffer [50 mM Tris·HCl (pH 7.5), 0.5 M NaCl, 5 mM EDTA, 1% Triton X-100, 1 mM PMSF, protease inhibitor mixture]. The beads were then washed and boiled in SDS/PAGE sample buffer. The eluents were analyzed by Silver Quest (Invitrogen) and candidate bands were subjected to mass spectrometry.

Organ Culture of the Metanephric Mesenchyme. Organ culture experiments were performed as described in refs. 7 and 8. Briefly, metanephroi were dissected from E11.5 embryos and the ureteric buds were removed after 5 min of incubation with 0.2% collagenase (Sigma). The mesenchyme rudiments were cultured on 3T3Wnt4 cells or L-Wnt9b cells at the air-fluid interface on a polycarbonate filter (0.4 μm; Corning) supplied with DMEM plus 10% FCS (3, 13, 14).

Generation of Cell Lines Expressing Tetracycline-Inducible Kif26b. The SalI-NotI fragment of Flag-tagged *Kif26b* was cloned into the EcoRV-NotI site of a pcDNA5/FRT/TO vector and transfected into Flp-In T-Rex HEK293 cells (Invitrogen). Stable transformants were selected following the manufacturer's instructions. All of the isolated clones showed identical induction of Kif26b in the presence of tetracycline (1 μg/mL). For inducible induction of *Kif26bΔC*, a 3.0-kb SalI-MluI fragment was cloned into the EcoRV site of the pcDNA5/FRT/TO vector. For dissociation assays, the cells were treated with 0.01% trypsin in Hepes-buffered calcium- and magnesium-free Puck's saline (HCMF) supplemented with 1 mM $CaCl_2$ (TC treatment) or 1 mM EDTA (pH 7.5) (TE treatment) for 15 min at 37 °C, respectively, followed by pipetting 10 times. The extent of the cell dissociation was represented by the index N_{TC}/N_{TE}, where N_{TC} and N_{TE} were the numbers of cell clusters after the TC and TE treatments, respectively (34). For NMHC II inhibition, 100 μg/mL (–)-blebbistatin (Calbiochem) and its negative control (+)-blebbistatin (Calbiochem) were used.

ACKNOWLEDGMENTS. We thank K. Shinmyozu and A. Nakamura for mass spectrometry; A. Nagafuchi, K. Oozono, J. Usui, M. Takeichi, M. A. Conti, and R. S. Adelstein for technical advice; M. Takasato and T. Ohmori for technical assistance; and L. F. Reichardt, N. D. Rosenblum, and A. P. McMahon for providing the anti-integrin α8 antibody, a protocol for cilia staining, and Wnt-expressing feeder cells, respectively. The monoclonal antibody against MYH10 developed by G. W. Conrad was obtained from the Developmental Studies Hybridoma Bank developed under the auspices of the National Institute of Child Health and Human Development (NICHD) and maintained by the University of Iowa. This work was supported in part by Grants-in-Aid from the Ministry of Education, Culture, Sports, Science, and Technology (MEXT) and the Global COE Program (Cell Fate Regulation Research and Education Unit, MEXT, Japan).

1. Müller U, et al. (1997) Integrin α8β1 is critically important for epithelial-mesenchymal interactions during kidney morphogenesis. *Cell* 88:603–613.
2. Linton JM, Martin GR, Reichardt LF (2007) The ECM protein nephronectin promotes kidney development via integrin α8β1-mediated stimulation of Gdnf expression. *Development* 134:2501–2509.
3. Carroll TJ, et al. (2005) Wnt9b plays a central role in the regulation of mesenchymal to epithelial transitions underlying organogenesis of the mammalian urogenital system. *Dev Cell* 9:283–292.
4. Nishinakamura R (2008) Stem cells in the embryonic kidney. *Kidney Int* 73:913–917.
5. Self M, et al. (2006) Six2 is required for suppression of nephrogenesis and progenitor renewal in the developing kidney. *EMBO J* 25:5214–5228.
6. Kobayashi A, et al. (2008) Six2 defines and regulates a multipotent self-renewing nephron progenitor population throughout mammalian kidney development. *Cell Stem Cell* 3:169–181.
7. Nishinakamura R, et al. (2001) Murine homolog of SALL1 is essential for ureteric bud invasion in kidney development. *Development* 128:3105–3115.
8. Osafune K, Takasato M, Kispert A, Asashima M, Nishinakamura R (2006) Identification of multipotent progenitors in the embryonic mouse kidney by a novel colony-forming assay. *Development* 133:151–161.
9. Takasato M, et al. (2004) Identification of kidney mesenchymal genes by a combination of microarray analysis and Sall1-GFP knockin mice. *Mech Dev* 121:547–557.
10. Miki H, Okada Y, Hirokawa N (2005) Analysis of the kinesin superfamily: Insights into structure and function. *Trends Cell Biol* 15:467–476.
11. Hirokawa N, Noda Y (2008) Intracellular transport and kinesin superfamily proteins, KIFs: Structure, function, and dynamics. *Physiol Rev* 88:1089–1118.
12. Yamashita K, Sato A, Asashima M, Wang PC, Nishinakamura R (2007) Mouse homolog of SALL1, a causative gene for Townes-Brocks syndrome, binds to A/T-rich sequences in pericentric heterochromatin via its C-terminal zinc finger domains. *Genes Cells* 12: 171–182.
13. Stark K, Vainio S, Vassileva G, McMahon AP (1994) Epithelial transformation of metanephric mesenchyme in the developing kidney regulated by Wnt-4. *Nature* 372: 679–683.
14. Kispert A, Vainio S, McMahon AP (1998) Wnt-4 is a mesenchymal signal for epithelial transformation of metanephric mesenchyme in the developing kidney. *Development* 125:4225–4234.
15. Majumdar A, Vainio S, Kispert A, McMahon J, McMahon AP (2003) Wnt11 and Ret/Gdnf pathways cooperate in regulating ureteric branching during metanephric kidney development. *Development* 130:3175–3185.
16. Conti MA, Adelstein RS (2008) Nonmuscle myosin II moves in new directions. *J Cell Sci* 121:11–18.
17. Nonaka S, et al. (1998) Randomization of left-right asymmetry due to loss of nodal cilia generating leftward flow of extraembryonic fluid in mice lacking KIF3B motor protein. *Cell* 95:829–837.
18. Corbit KC, et al. (2008) Kif3a constrains beta-catenin-dependent Wnt signalling through dual ciliary and non-ciliary mechanisms. *Nat Cell Biol* 10:70–76.
19. Lin F, et al. (2003) Kidney-specific inactivation of the KIF3A subunit of kinesin-II inhibits renal ciliogenesis and produces polycystic kidney disease. *Proc Natl Acad Sci USA* 100:5286–5291.
20. Singla V, Reiter JF (2006) The primary cilium as the cell's antenna: Signaling at a sensory organelle. *Science* 313:629–633.
21. Yu J, Carroll TJ, McMahon AP (2002) Sonic hedgehog regulates proliferation and differentiation of mesenchymal cells in the mouse metanephric kidney. *Development* 129:5301–5312.
22. Zhou R, Niwa S, Homma N, Takei Y, Hirokawa N (2009) KIF26A is an unconventional kinesin and regulates GDNF-Ret signaling in enteric neuronal development. *Cell* 139: 802–813.
23. Conti MA, Even-Ram S, Liu C, Yamada KM, Adelstein RS (2004) Defects in cell adhesion and the visceral endoderm following ablation of nonmuscle myosin heavy chain II-A in mice. *J Biol Chem* 279:41263–41266.
24. Ma X, Bao J, Adelstein RS (2007) Loss of cell adhesion causes hydrocephalus in nonmuscle myosin II-B-ablated and mutated mice. *Mol Biol Cell* 18:2305–2312.
25. Lillie SH, Brown SS (1994) Immunofluorescence localization of the unconventional myosin, Myo2p, and the putative kinesin-related protein, Smy1p, to the same regions of polarized growth in Saccharomyces cerevisiae. *J Cell Biol* 125:825–842.
26. Beningo KA, Lillie SH, Brown SS (2000) The yeast kinesin-related protein Smy1p exerts its effects on the class V myosin Myo2p via a physical interaction. *Mol Biol Cell* 11: 691–702.
27. Linask KK, Manisastry S, Han M (2005) Cross talk between cell-cell and cell-matrix adhesion signaling pathways during heart organogenesis: Implications for cardiac birth defects. *Microsc Microanal* 11:200–208.
28. Lu W, et al. (2008) Cellular nonmuscle myosins NMHC-IIA and NMHC-IIB and vertebrate heart looping. *Dev Dyn* 237:3577–3590.
29. Teng J, et al. (2005) The KIF3 motor transports N-cadherin and organizes the developing neuroepithelium. *Nat Cell Biol* 7:474–482.
30. Murata T, et al. (2004) ang is a novel gene expressed in early neuroectoderm, but its null mutant exhibits no obvious phenotype. *Gene Expr Patterns* 5:171–178.
31. Sakaki-Yumoto M, et al. (2006) The murine homolog of SALL4, a causative gene in Okihiro syndrome, is essential for embryonic stem cell proliferation, and cooperates with Sall1 in anorectal, heart, brain and kidney development. *Development* 133:3005–3013.
32. Kobayashi H, Kawakami K, Asashima M, Nishinakamura R (2007) Six1 and Six4 are essential for Gdnf expression in the metanephric mesenchyme and ureteric bud formation, while Six1 deficiency alone causes mesonephric-tubule defects. *Mech Dev* 124:290–303.
33. Sato Y, et al. (2009) Molecular basis of the recognition of nephronectin by integrin alpha8beta1. *J Biol Chem* 284:14524–14536.
34. Nagafuchi A, Ishihara S, Tsukita S (1994) The roles of catenins in the cadherin-mediated cell adhesion: Functional analysis of E-cadherin-alpha catenin fusion molecules. *J Cell Biol* 127:235–245.

Cell Stem Cell
Brief Report

Generation of Induced Pluripotent Stem Cells from Human Terminally Differentiated Circulating T Cells

Tomohisa Seki,[1,7] Shinsuke Yuasa,[1,2,7] Mayumi Oda,[2] Toru Egashira,[1] Kojiro Yae,[1] Dai Kusumoto,[1] Hikari Nakata,[1] Shugo Tohyama,[1] Hisayuki Hashimoto,[1] Masaki Kodaira,[1] Yohei Okada,[2,3] Hiroyuki Seimiya,[4] Noemi Fusaki,[5,6] Mamoru Hasegawa,[5] and Keiichi Fukuda[1,*]
[1]Department of Cardiology
[2]Center for Integrated Medical Research
[3]Department of Physiology
Keio University School of Medicine, Tokyo 160-8582, Japan
[4]Division of Molecular Biotherapy, Cancer Chemotherapy Center, Japanese Foundation for Cancer Research, Tokyo 135-8550, Japan
[5]DNAVEC Corporation, Ibaraki 1-25-11, Japan
[6]PRESTO, JST, Saitama 332-0012, Japan
[7]These authors contributed equally to this work
*Correspondence: kfukuda@sc.itc.keio.ac.jp
DOI 10.1016/j.stem.2010.06.003

The direct reprogramming of somatic cells to produce induced pluripotent stem cells (iPSCs) is a prominent recent advance in stem cell biology (Takahashi and Yamanaka, 2006). Generation of iPSCs without genomic integration of extrinsic genes is highly desirable. Initially, human dermal fibroblasts were used to derive human iPSCs (hiPSCs) (Takahashi et al., 2007; Yu et al., 2007). However, recent studies have shown that other human somatic stem cells can be used (Aasen et al., 2008; Eminli et al., 2009; Kim et al., 2009; Ye et al., 2009). It is difficult to obtain human somatic stem cells, but human terminally differentiated circulating T cells (hTDCTCs) are readily available from peripheral blood. Here, we show that a combination of activated T cell cultivation and a temperature-sensitive mutated Sendai virus (SeV) that encodes human OCT3/4, SOX2, KLF4, and c-MYC allows the generation of hiPSCs easily, efficiently, and safely within a 1 month time frame.

Sampling of peripheral blood is one of the least invasive procedures performed routinely in clinics, and surplus peripheral blood samples are often left unused after clinical examinations. Among peripheral blood mononuclear cells (PBMCs), T cells can be readily cultured in vitro by means of a plate-bound anti-CD3 monoclonal antibody and recombinant (r)IL-2 (Desai-Mehta et al., 1996), and we used such an approach to expand hTDCTCs from peripheral blood samples. From 1 ml of whole blood, PBMCs were separated on a Ficoll gradient and then cultured with plate-bound anti-CD3 monoclonal antibody and rIL-2 (Figure 1A). Although PBMC fractions contain lymphocytes and monocytes, T cells are selectively cultured under these conditions. In culture, the number of activated T cells increased gradually but consistently. Five days after blood sampling, the cultured cells were morphologically identical to pure CD3-positive T cells collected by fluorescence-activated cell sorting (FACS) (Figure 1B). We used a whole-PBMC culture method because it is technically simpler than FACS, in which the sorted cells are frequently damaged by laser emission and the process of single-cell sorting.

To avoid transgene integration during iPSC generation, we used an SeV vector, which is a minus-strand RNA virus that is not integrated into the host genome and is not pathogenic for humans (Li et al., 2000). We used a temperature-sensitive mutated SeV vector in these experiments to reduce transgene expression and SeV residue in generated lines. This form of SeV vector generates weaker transgene expression and cannot proliferate at standard culture temperatures (data not shown). SeV can be efficiently transduced into human T cells and can express exogenous genes (Okano et al., 2003). We first introduced green fluorescent protein (GFP) into human T cells by SeV in a dose-dependent manner; toxicity for the infected cells was minimal at the virus dosages used (Figure 1C). To generate iPSCs from hTDCTCs, we used SeV to deliver multiple transgenes that encoded stem cell-specific transcription factors, such as *OCT3/4*, *SOX2*, *KLF4*, and *c-MYC*, into cells on day 6 of culture. Two days after gene introduction, the cells were replated onto feeder layers of SNL cells. On day 9, the cells were transferred to human ES cell (ESC) medium that contained 4 ng/ml bFGF. Within 3 weeks of infection, we identified a colony that resembled human ESCs (hESCs) among the T cell derivatives. On day 25, colonies that were larger and morphologically similar to hESC-like colonies were picked (Figure 1D). Of these initial colonies, which were identified by crystal violet staining, most were positive for alkaline phosphatase (ALP), which is a characteristic marker of stem cells (Figure 1E). T cells that had been transfected with SeV vectors carrying *OCT3/4, SOX2, KLF4,* and *c-MYC* were plated onto mitomycin C-treated SNL feeder cells at 5×10^4 cells per 10 cm dish. Around day 25 after blood sampling, the number of ALP-positive hESC-like colonies was counted and approximately 50 colonies were observed at MOI 20 (Figure 1E) (an efficiency of 0.1%). Moreover, the efficiency of iPSC colony generation was dependent upon the dosage of virus used for gene introduction (Figure 1F). We named these established T cell-derived iPSCs as "TiPS cells (TiPSCs)." After expansion, the cloned TiPSCs displayed typical hESC/iPSC morphology and had a normal karyotype (Figures S1A and S1B available online).

To confirm that the TiPSCs had the characteristics of typical ESC/iPSCs, we

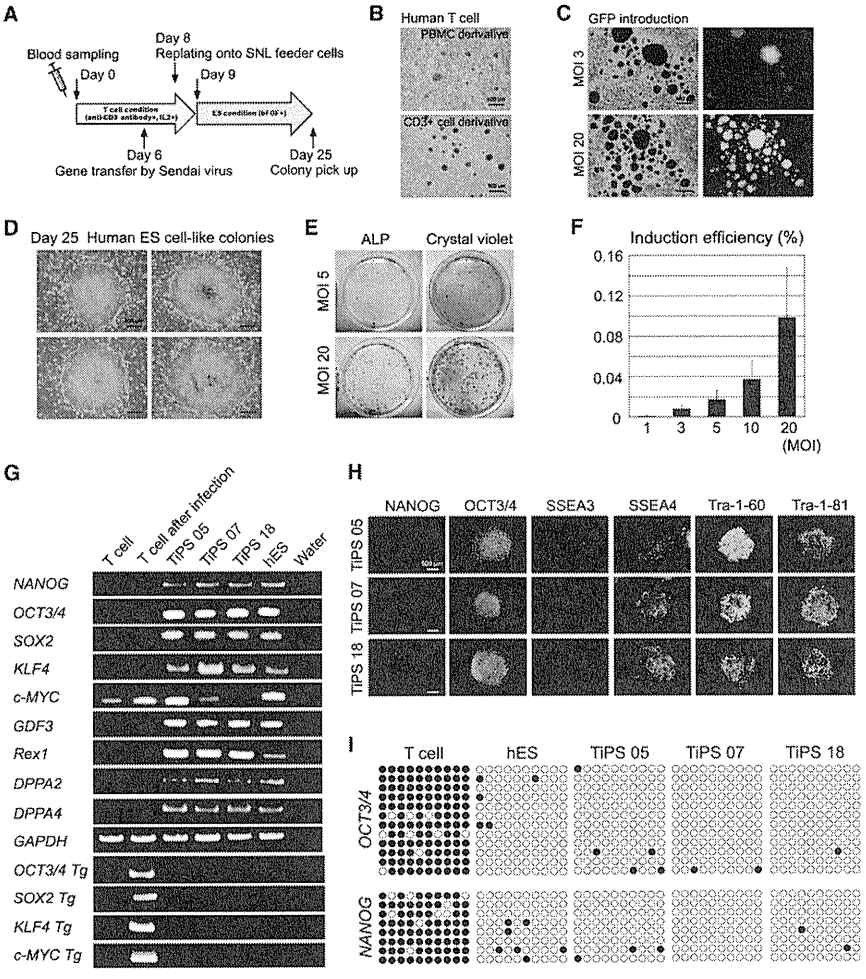

Figure 1. hTDCTCs-Derived iPSC Colonies

(A) Strategy used in the present study for reprogramming T cells.

(B) Morphologies of T cells derived from whole PBMCs or FACS-sorted T cells grown in the presence of CD3 antibody and rIL2.

(C) Efficient GFP introduction by SeV in T cells transfected at an MOI of 3 or MOI of 20.

(D) Typical ESC-like iPSC colonies on day 25 after blood sampling.

(E) Examples of 10 cm dishes stained for ALP on day 25, showing numerous ALP-positive colonies of T cells that were transfected at an MOI of 5 or MOI of 20.

(F) Numbers of ALP-positive colonies in relation to multiplicity of infection.

(G) RT-PCR analyses for the hESC marker genes *NANOG*, *OCT3/4*, *SOX2*, *KLF4*, *c-MYC*, *GDF3*, *REX1*, *DPPA2*, and *DPPA4* and the transgenes *OCT3/4*, *SOX2*, *KLF4*, and *c-MYC*.

(H) Immunofluorescence staining for pluripotency and surface markers (NANOG, OCT3/4, SSEA3, SSEA4, TRA-1-60, and TRA-1-81) in TiPS 05, 07, and 18. Scale bars represent 500 μm.

(I) Bisulfite sequencing analysis of the *NANOG* and *OCT3/4* promoter regions in peripheral T cells, hESCs, and hTiPSCs 05, 07, and 18. Each row of circles for a given amplicon represents the methylation status of the CpG dinucleotides in one bacterial clone for that region. Open circles represent unmethylated CpGs; closed circles represent methylated CpGs.

See also Figure S1 and Table S1.

examined stem cell marker expression. Reverse-transcription PCR (RT-PCR) analyses revealed that the TiPS 05, 07, and 18 clones expressed ESC marker transcripts for *NANOG*, *OCT3/4*, *SOX2*, *KLF4*, *c-MYC*, *GDF3*, *REX1*, *DPPA2*, and *DPPA4*. The original T cells also expressed *c-MYC* at a basal level, as previously reported (Douglas et al., 2001). In the TiPSCs, the *OCT3/4*, *SOX2*, *KLF4*, and *c-MYC* transgenes were lost after several passages (Figure 1G; Figure S1C). Immunostaining revealed that the TiPSCs expressed the Nanog, Oct3/4, SSEA3, SSEA4, Tra-1-60, and Tra-1-81 proteins (Figure 1H). High telomerase activity is also an important characteristic of iPSCs, and, appropriately, TiPSCs showed high levels of telomerase activity (Figure S1D). Another signature of iPSCs is epigenetic remodeling. We used bisulfite sequencing to examine the methylation status of the *NANOG* and *OCT3/4* promoters. T cells, which do not express *NANOG* or *OCT3/4*, showed mostly methylated CpGs in those promoters. hESCs, which do express *NANOG* and *OCT3/4*, showed unmethylated CpGs in those promoters. As in hESCs, the CpGs in these promoter regions were predominantly unmethylated in the TiPSCs (Figure 1I). These results suggest that SeV-mediated gene transfer successfully reprograms hTDCTCs.

Somatic recombination of T cell receptor (TCR) genes generates a diverse T cell repertoire that allows adaptation for antigen responses (Krangel, 2009). To confirm that the TiPSCs were derived from hTDCTCs, we analyzed TCR rearrangements. A hallmark of the TCR-β locus is developmentally ordered recombination, with Dβ-to-Jβ recombination preceding Vβ-to-DβJβ recombination. We performed capillary electrophoresis of the PCR products for the genomic DNA of the TCR-β regions. As a positive control, we used monoclonal T cells, which are derived from patients with lymphocyte malignancies and show a specific peak, because these T cells have only a single genetic variation in their TCR regions (Figure S2A). Peripheral T cells from people without lymphocytic diseases are polyclonal, with diverse genetic variations in their TCR rearrangements, and show a broad and low band without a specific peak. ESCs do not have TCR rearrangements and do not show a specific positive peak. The TiPS 05, 07, and 18 cell lines showed specific peaks for Dβ/Jβ recombination. TiPS 05 showed Vβ/Jβ2 recombination. TiPS 07 and TiPS 18 showed Vβ/Jβ1,2 recombination, albeit with different bands (Figure 2A). TCR rearrangement is specific for T cell development, so these results confirm that TiPSCs are derived from T cells. They also indicate that the TiPS 05, 07, and 18 lines originated from different T cells. We analyzed the rearrangement pattern of 10 independent TiPSCs and confirmed that every TiPSCs showed different rearrangement pattern (Figure S2A).

We also performed global gene expression analyses with DNA chips. Scatter plot analyses revealed global gene

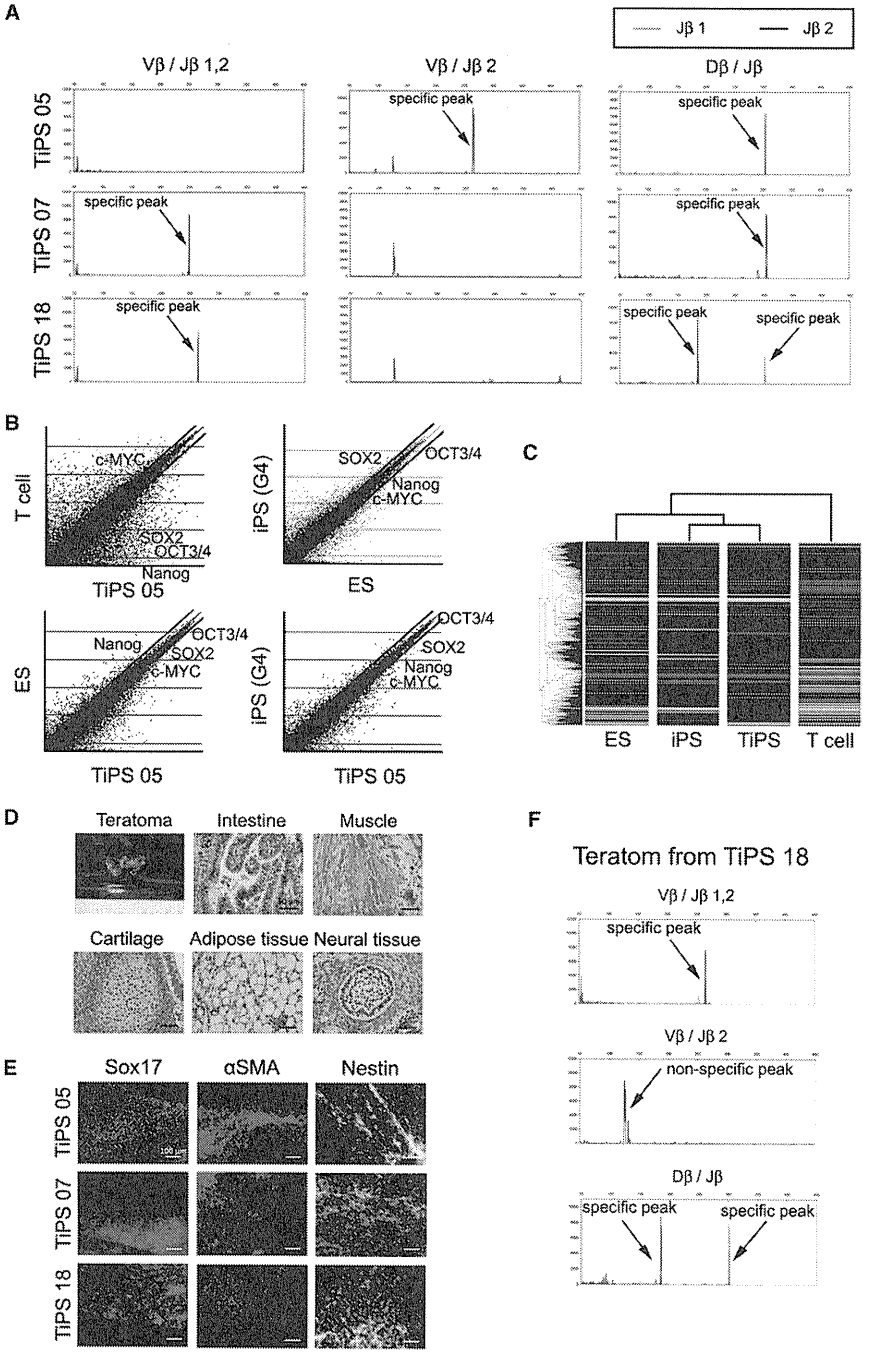

Figure 2. Detail Characterizations of TiPSCs

(A) Characterization of the TCR-β rearrangement by capillary electrophoresis. The green line is derived from the band for the Jβ1 gene, and blue line is derived from the band for the Jβ2 gene. TiPS 05 shows rearrangements of Vβ/Jβ2 and Dβ/Jβ. TiPS 07 shows rearrangements of Vβ/Jβ1,2 and Dβ/Jβ. TiPS 18 shows rearrangements of Vβ/Jβ1,2 and Dβ/Jβ.

(B) Scatter plots comparing the global gene expression profiles of T cells and TiPS cells, dermal fibroblast-derived iPSCs (G4) and ESCs, ESCs and TiPSCs, and dermal fibroblast-derived iPSCs (G4) and TiPSCs. The black lines indicate 2-fold differences in gene expression levels between the paired cell populations. The transcript expression levels are shown on a $\log_2$ scale. The expression levels of *NANOG*, *OCT3/4*, *SOX2*, and *c-MYC* are shown.

(C) Heat map analyses of hESCs, dermal fibroblast-derived iPSCs, TiPSCs, and the parental human T cells.

(D) Gross morphology, hematoxylin and eosin-stained representative teratomas derived from TiPS 05.

(E) Immunofluorescence staining for Sox17 (endodermal marker), αSMA (mesodermal marker), and Nestin (ectodermal marker) in each TiPSC-derived differentiated cell.

(F) Characterization of the TCR-β rearrangement for teratoma from TiPS 18.

See also Figure S2 and Table S2.

expression differences between peripheral T cells and TiPSCs. Comparison of hESCs and human dermal fibroblast-derived iPSCs, hESCs, and human TiPSCs (hTiPSCs), and dermal fibroblast-derived iPSCs and TiPSCs showed high levels of similarity (Figure 2B). Heat map analysis showed that the global gene expression profiles were overall similar in ESCs, dermal fibroblast-derived iPSCs, and TiPSCs, and different from T cells (Figure 2C). To further demonstrate the pluripotency of hTiPSCs, they were transplanted into the subcutaneous tissue of severe combined immunodeficient (SCID) mice. Six to eight weeks after injection, each TiPSC line tested gave rise to teratomas that contained derivatives of all three germ layers (Figure 2D; Figure S2B). We also examined the in vitro differentiation potential of TiPSCs. Each TiPSC line tested generated embryoid bodies that contained derivatives of all three germ layers (Figure 2E). These results indicate that hTiPSCs are pluripotent stem cells. Although it was reported that Trp53 null murine T cells could be reprogrammed into iPSCs (Hong et al., 2009), we have successfully reprogrammed wild-type human T cells. In our hands, the efficiency of conventional retrovirus-mediated gene transfer into wild-type human T cells was very low compared to SeV (data not shown). In our view, the efficiency of gene transfer is a major determining factor in successful iPSC generation.

With current technology, if iPSC-derived mature cells are transplanted into diseased patients, there is no good procedure for following their progeny, which could eventually form malignant or benign tumors. In animal models, several marker genes can be used to chart the progression and consequences of iPSC-derived mature cell transplantation, such as GFP and luciferase. However, it is not desirable to insert exogenous marker genes into the genomes of hiPSCs for clinical use. TiPSCs, however, already have a traceable genetic signature through TCR locus rearrangement. Consistent with this idea, teratomas derived from TiPSCs had

same signature as undifferentiated TiPSCs (Figure 2F; Figure S2C). Therefore, the descendents of TiPSCs can be identified by analyzing their TCR rearrangement patterns.

In conclusion, we have developed a minimally invasive method for hiPSC generation without genomic integration that uses low numbers of hTDCTCs from peripheral blood. This method has advantages for research into stem cell reprogramming, TCR rearrangement, immunologic disorders, and the development of genetic markers for future applications of regenerative medicine. TiPSCs may well be relatively easy to use in a clinical setting.

ACCESSION NUMBERS

The microarray data have been deposited in GEO and given the series accession number GSE22088.

SUPPLEMENTAL INFORMATION

Supplemental Information includes Supplemental Experimental Procedures, two figures, and two tables and can be found with this article online at doi:10.1016/j.stem.2010.06.003.

ACKNOWLEDGMENTS

This study was supported in part by research grants from the project for realization of regenerative medicine, the Ministry of Education, Science, and Culture, Japan, and by a grant from the New Energy and Industrial Technology Development Organization (NEDO). We thank Dr. Kyotaro Hirashima for technical assistance with TRAP assay. N.F. is an employee of DNAVEC Corporation and M.H. is a founder and shareholder of DNAVEC Corporation

Received: May 5, 2010
Revised: June 3, 2010
Accepted: June 5, 2010
Published: July 1, 2010

REFERENCES

Aasen, T., Raya, A., Barrero, M.J., Garreta, E., Consiglio, A., Gonzalez, F., Vassena, R., Bilic, J., Pekarik, V., Tiscornia, G., et al. (2008). Nat. Biotechnol. *26*, 1276–1284.

Desai-Mehta, A., Lu, L., Ramsey-Goldman, R., and Datta, S.K. (1996). J. Clin. Invest. *97*, 2063–2073.

Douglas, N.C., Jacobs, H., Bothwell, A.L., and Hayday, A.C. (2001). Nat. Immunol. *2*, 307–315.

Eminli, S., Foudi, A., Stadtfeld, M., Maherali, N., Ahfeldt, T., Mostoslavsky, G., Hock, H., and Hochedlinger, K. (2009). Nat. Genet. *41*, 968–976.

Hong, H., Takahashi, K., Ichisaka, T., Aoi, T., Kanagawa, O., Nakagawa, M., Okita, K., and Yamanaka, S. (2009). Nature *460*, 1132–1135.

Kim, J.B., Greber, B., Arauzo-Bravo, M.J., Meyer, J., Park, K.I., Zaehres, H., and Scholer, H.R. (2009). Nature *461*, 649–653.

Krangel, M.S. (2009). Curr. Opin. Immunol. *21*, 133–139.

Li, H.-O., Zhu, Y.-F., Asakawa, M., Kuma, H., Hirata, T., Ueda, Y., Lee, Y.-S., Fukumura, M., Iida, A., Kato, A., et al. (2000). J. Virol. *74*, 6564–6569.

Okano, S., Yonemitsu, Y., Nagata, S., Sata, S., Onimaru, M., Nakagawa, K., Tomita, Y., Kishihara, K., Hashimoto, S., Nakashima, Y., et al. (2003). Gene Ther. *10*, 1381–1391.

Takahashi, K., and Yamanaka, S. (2006). Cell *126*, 663–676.

Takahashi, K., Tanabe, K., Ohnuki, M., Narita, M., Ichisaka, T., Tomoda, K., and Yamanaka, S. (2007). Cell *131*, 861–872.

Ye, Z., Zhan, H., Mali, P., Dowey, S., Williams, D.M., Jang, Y.-Y., Dang, C.V., Spivak, J.L., Moliterno, A.R., and Cheng, L. (2009). Blood *114*, 5473–5480.

Yu, J., Vodyanik, M.A., Smuga-Otto, K., Antosiewicz-Bourget, J., Frane, J.L., Tian, S., Nie, J., Jonsdottir, G.A., Ruotti, V., Stewart, R., et al. (2007). Science *318*, 1917–1920.

Note Added in Proof

A manuscript has appeared online demonstrating isolation of iPSCs from peripheral blood, including a single line that showed evidence for both TCR-β and TCR-γ rearrangement by PCR (Kunisato, A., Wakatsuki, M., Shinba, H., Ota, T., Ishida, I., and Nagao, K. [2010]. Direct generation of induced pluripotent stem cells from human non-mobilized blood. Stem Cells Dev., in press. Published online May 24, 2010. 10.1089/scd.2010.0063).